Copyright Warning & Restrictions

The copyright law of the United States (Title 17, United States Code) governs the making of photocopies or other reproductions of copyrighted material.

Under certain conditions specified in the law, libraries and archives are authorized to furnish a photocopy or other reproduction. One of these specified conditions is that the photocopy or reproduction is not to be "used for any purpose other than private study, scholarship, or research." If a, user makes a request for, or later uses, a photocopy or reproduction for purposes in excess of "fair use" that user may be liable for copyright infringement,

This institution reserves the right to refuse to accept a copying order if, in its judgment, fulfillment of the order would involve violation of copyright law.

Please Note: The author retains the copyright while the New Jersey Institute of Technology reserves the right to distribute this thesis or dissertation

Printing note: If you do not wish to print this page, then select "Pages from: first page # to: last page #" on the print dialog screen

ABSTRACT

A NEW CONCEPT IN ARTIFICIAL LIGAMENT AND TENDONS MODELING: FINITE ELEMENT ANALYSIS

by
Miroslaw Sokol

Reconstruction of the Anterior Cruciate Ligament (ACL) has been a major focus in sports medicine for over twenty years. Severe or unrepairable damage of the ACL due to sport injury is a major problem faced by orthopedic surgeons and engineers. To successfully replace or reconstruct an injured ACL, the mechanical properties as well as the dimensional limitation of the material used must be similar to the biological ligaments. Although excessive literature describes experimental investigation on the mechanical property and clinical application of the ligament material, there is no analytical study that describes strains, stresses, and endurance in the bone/ligament/bone complex. The Finite Element Analysis (FEA) is a method to study this problem. The objectives of the present investigation are (1) to develop a finite element model (FEM) of an artificial ligament yarn, the emphasis is put on the development of the elastic FEM, (2) to analyze stress distribution in the ligament yarn fibers due to various loading conditions and designs, and (3) to compare results obtained from the FEA of the elastic model with results obtained from laboratory tensile test. Results obtained from the FEM model of the ACL prosthesis yarn are confirmed by experimental measurements.

A NEW CONCEPT IN ARTIFICIAL LIGAMENT AND TENDONS MODELING: FINITE ELEMENT ANALYSIS

by
Miroslaw Sokol

A Thesis
Submitted to the Faculty of
New Jersey Institute of Technology
in Partial Fulfillment of the Requirements for the Degree of
Master in Science in Biomedical Engineering

Biomedical Engineering Committee

May 1996

APPROVAL PAGE

A NEW CONCEPT IN ARTIFICIAL LIGAMENT AND TENDONS MODELING: FINITE ELEMENT ANALYSIS

by
Miroslaw Sokol

Tai-Ming (Tina) Chu, Ph.D., Thesis Advisor — Date
Assistant Professor of Mechanical Engineering, NJIT

Bernard Koplik, Ph.D., Committee Member — Date
Chairman and Professor of Mechanical Engineering, NJIT

Edward Wong, Ph.D., Committee Member — Date
Assistant Director - Scientific Affairs, Howmedica Inc., Worldwide R&D

BIOGRAPHICAL SKETCH

Author: Miroslaw Sokol

Degree: Master of Science in Biomedical Engineering

Date: May 1996

Graduate Education:

- Master of Science in Biomedical Engineering
  New Jersey Institute of Technology
  Newark, New Jersey, 1996

- Master of Science in Mechanical Engineering
  Warsaw Institute of Technology
  Warsaw, Poland, 1986

Major: Biomedical Engineering

Publications:

1. Jezierski, J. & Sokol, M., The Theoretical Foundation of Selection in Dimensional Multi-Chain Links. *Mechanic*, (1990) 14-30.

2. Kacprzyk, Z., Maj, M., Pawlowska, B., Sokol, M. & Sokol, T., The Finite Element Analysis System - Theoretical Handbook. *Warsaw Institute of Technology Press*, (1990).

ACKNOWLEDGMENT

I would like to express my genuine gratitude to my thesis adviser professor Tai-Ming (Tina) Chu for her guidance, suggestion, and help through this research. Her supervision and support were an invaluable contribution and had influenced to complete organization of my work.

I would like to thank Howmedica Inc., Worldwide R&D for allowing me to use experimental data to support results obtained from analytical model of ligament material. I would like to thank DR. Edward Wong for discussion and comments on this thesis and also professor Bernard Koplik for serving as a committee member.

Finally, I want to thank my wife Alicja Stec, Bupendra Patel, Aaron Essner, and DR. Aigou Wang for their help and encouragement.

TABLE OF CONTENTS

TABLE OF CONTENTS
(Continued)

TABLE OF CONTENTS
(Continued)

LIST OF FIGURES

LIST OF FIGURES
(Continued)

LIST OF FIGURES
(Continued)

Figure **Page**

LIST OF TABLES

TABLE OF SYMBOLS

A_f - filament area,

A_t - yarn area,

b - contact area radius,

E - Young modulus,

E_1, E_2 - Young modulus for first and second cylinders respectively,

G - Kirchoff constant,

η - contact stiffness,

κ - radius of filament curvature,

l - length of the twisted segment,

l_1 - initial filament section length,

l_2 - final filament section length,

n - number of filaments in the yarn,

ν_1, ν_2 - Poisson's ratio,

P - contact pressure,

θ - internal filament rotation angle,

θ_f - filament twisting angle,

r - distance between the yarn's and filament's symmetry axis,

R_1, R_2 - cylinder radius,

R_f - filament radius,

R_t - average yarn radius,

σ_{max} - maximum contact stress,

t - parameter.

CHAPTER 1

INTRODUCTION

1.1 Problems in the Anterior Cruciate Ligament Deficient Knee

Reconstruction of anterior cruciate ligament (ACL) in deficient knee has been a major focus in sports medicine research over the past 20 years. The number of knee and ankle ligament injuries in sports and traffic accidents increases continuously. The need for a functional stability and preventing the potential for a development of arthritis in the ACL deficient knee has led to the usage of inter articlular autogenous reconstruction from multiple tissue sources. This transplant requires to sacrifice a tendon or ligament with a normal biological function. In many cases autogenous tissue may not be available or its quality is poor when previous autogenous reconstruction has failed.

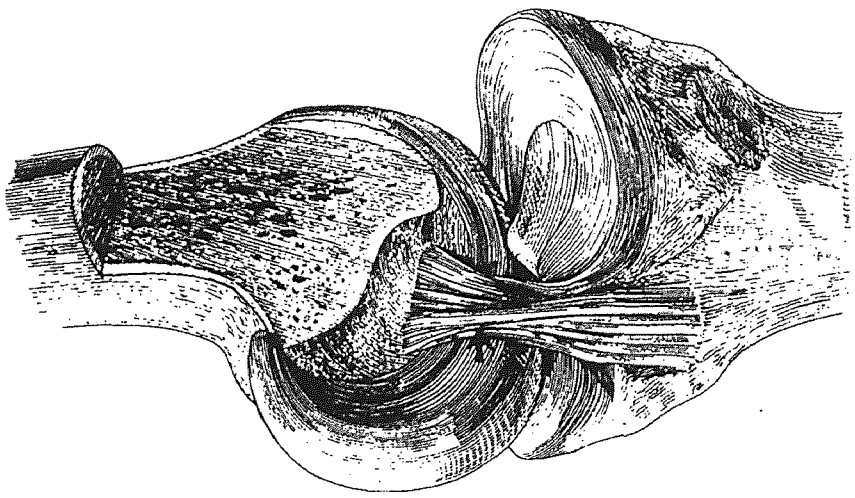

Figure 1.1.1 Anterior Cruciate Ligament [4]

Therefore, the only alternative is the synthetic or prosthetic ligament device. The operative treatment is required only for complete rupture of a ligament with proven instability. The method of reconstruction uses the central one third portion of the patella tendon and tibia tubercle. This has been the standard reconstruction method. Other common tissue sources for ACL reconstruction such as semi-tendinosus, gracilis, and the fascia lata graft, have been used in a number of varied techniques. Unfortunately, procedures for the replacing of ligaments with autogenous and allogeneic material such as tendons or fascia lata and with alloplastic material have led to unfavorable results in many cases. Studies have shown that the original strength of autogenous tissue declines with time. The original strength of material used for implants, in many cases, fails to fully return to the original condition. In addition, there is a great variability in healing and revascularization.

1.2 Synthetics Material Used in Anterior Cruciate Ligament Reconstruction

The use of a synthetic material for anterior cruciate ligament (ACL) reconstruction was first reported in 1918. Alwyn-Smith attempted to use silk sutures as a replacement of ACL.[1] In the early seventies, a clinical trial of Proplast an ACL prosthesis was initialized.[2, 3] This prosthesis was used for both anterior and posterior cruciate ligament replacement.

There are several objectives for use of an artificial material in ACL reconstruction. The prosthetic ACL is easy to implant with minimum trauma. It gives immediate joint mobility, thus avoiding the degenerative events associated with joint immobility. It also simulates physical restrain system as the natural ACL (including stiffness). The

prosthetic anterior cruciate ligament provides long term biological compatibility with intracellular and extracellular environment.

In seventies and eighties, synthetic fibrous material was popular to use among the orthopedic surgeons. Synthetic replacement of the ACL may temporarily or permanently function as an augmentation device, a stent, a scaffold, or a total prosthesis.

Table 1.2.1 Classification of Commercially Available Cruciate Ligaments [3].

ACL replacement type	Brand name
Augmentation Device	LAD (fixed at one end) Versigraft (Carbon fiber composite stent) Suture: Dexon, Victyl, P.D.S.
Stent	Proplast LAD (fixed at both ends) Dacron
Scaffold	Carbon Fiber Leeds-Keio Stryker-Meadox Dacron™ Graft
Total Prosthesis	Surgicraft ABC Ligastic Gore-Tex Richards Polyethylene Ligament Swiss Polyethylene Ligament Stryker-Meadox Dacron™ Graft

An augmentation device is primarily intended to add strength to a biological graft as it undergoes degradation and revascularization. It provides load shearing between the biological tissue and the host tissue. One of the problems with an augmentation device is that it may stress shield the autogenous tissue, thus, prevents the tissue from developing adequate tensile strength. This may be avoided by fixing the synthetic material at only one end. For example, use the Kennedy Ligament Augmentation Device - LAD (Figure

1.2.1), 3M, St. Paul Minnesota, or a temporary biodegradable augmentation device, or a carbon fiber composite stent. If an augmentation device is fixed at both ends, it will function as a stent. The stent protects the graft from stress but usually stress shields tissue excessively if left inside permanently.

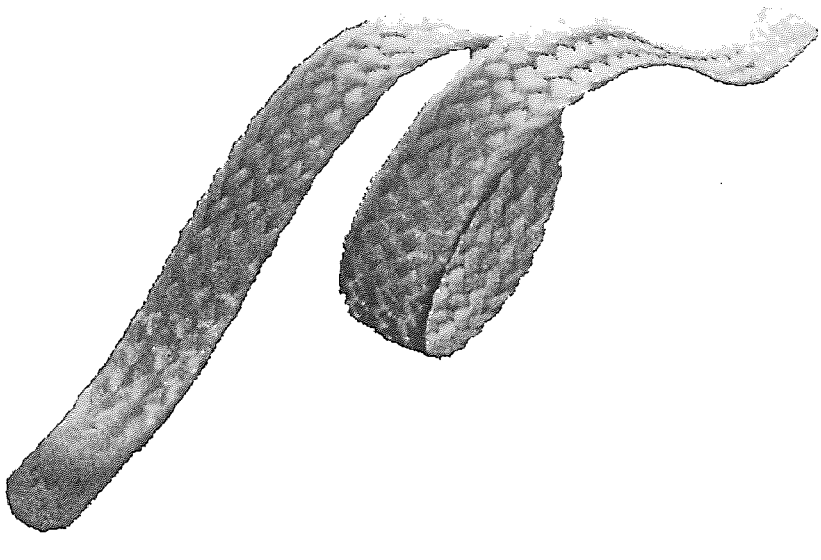

Figure 1.2.1 Kennedy Augmentation Device. Minnesota Mining and Manufacturing Company (1987).

A scaffold is used to provide support and it serves as a foundation for a soft tissue in growth. In some cases, scaffold may be permanent and augment the overall strength of the graft, for example, Stryker-Meadox Dacron, Leeds-Keio (Figures 1.3.1 and 1.2.2). Additionally, the scaffold is used, but gradually degenerates so it can be replaced by host tissue like carbon fiber. The initial strength of the scaffold should be adequate to provide biomechanical stability of the joint while the host collagen is produced and organized. Problems commonly associate with the scaffold include the variability of tissue to

withstand the required mechanical stress, and premature degradation of the synthetic material.

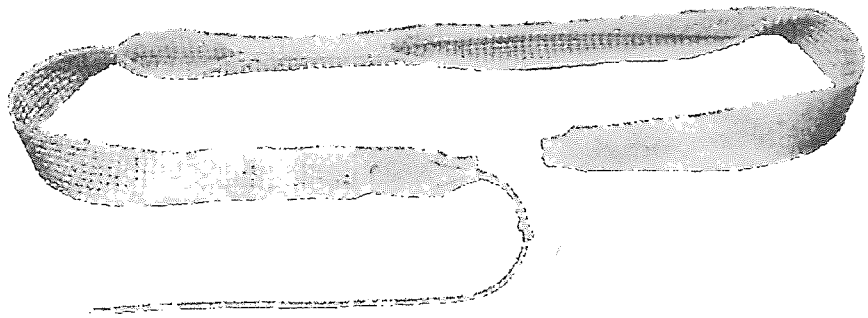

Figure 1.2.2 The tabular Leeds-Keio artificial ligament. [5]

The total prosthesis (Table 1.2.1) is a permanent implant that completely replaces the ACL without any soft tissue in growth. One of the problems associated with total prosthesis is lack of reproducibility of biomechanical function of Anterior Cruciate Ligament. High stiffness of total ACL prosthesis leads to the reduction of knee motion range and wear problems.

1.3 Application of Synthetics in ACL Replacement

Kennedy Ligament Augmentation Device (LAD) is used as an augmentation as well as a stent for ACL replacement. This product is made by 3M Orthopedic Product Division. This ligament is made out of braided polypropylene. During surgery, it is wrapped by a portion of the quadriceps tendon and rounded through the joint or over the top of the femoral condyle. The ultimate tensile strength of these ligaments are 1730 [N] for 8 [mm] and 1500 [N] for 6 [mm] devices. Fatigue strength is reduced 9 percent after 1 million

load cycles (50-500 [N]). The ligament elongates 4 percent after 1 million cycles with the same loading conditions. The authors indicated that, the earlier clinical results showed a high post-surgery composite ultimate tensile strength, tissue revascularization, and collagen remodeling.

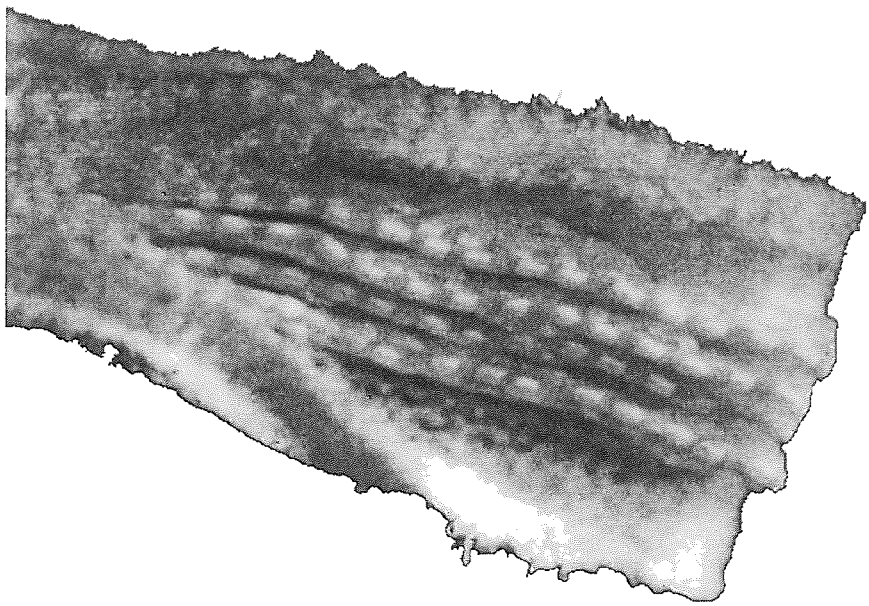

Figure 1.3.1 Stryker-Meadox Dacron™ Graft
Meadox Medical Inc. Oakland (1983).

Stryker Dacron™ Ligament (Figure 1.3.1) and Leeds-Keio Ligament System (Figure 1.2.2) are examples of scaffolds. Both prosthetic devices are designed to provide necessary initial tensile strength and allow the fibrous tissue ingrowth. The ultimate tensile strength of Stryker Dacron™ Ligament is about 3000 [N], one and half times more than human ACL. This prosthesis is also four times stiffer than human ACL. The originality of the Leeds-Keio Ligament System introduced by Howmedica International lies in the way the ligament is attached to the bone. In this prosthetic device, tibial and

femoral fixations are made by introducing a bone plug within a pouch in the implant after drawing it from tibial and femoral tunnels. The ultimate tensile strength of this ligament lies with in 2000 [N] range. The fatigue life is estimated on the 63 million cycles with 500 [N] load.

A typical example of total ligament prosthesis is the Gore-Tex Anterior Cruciate Ligament Prosthesis. This prosthesis is made out of polytetrafluoro-ethylene. The mechanical and biomechanical properties of this prosthetic device are summarized as follows. Ultimate tensile strength of the ligament is 5300 [N] (natural human ligament tensile strength is 2000 [N]) and has 8 - 10 percent of ultimate elongation. The cyclic creep test shows only 4 percent of permanent elongation after 34 million load cycles. The 25 percent reduction of ultimate tensile strength was observed after 84 million cycles of the bending fatigue test. The bending test was performed under 111 [N] of constant force with 30^0 of flexion over 1.5 [mm] radius edge corner.

1.4 Mathematical Modeling of Ligament and Tendon

Although a Finite Element Model (FEM) for solving problem involving the mechanical behavior of the ligament and tendon tissue does not exist, several mathematical models have been proposed. A mathematical model of the tendon and the ligament is studied by Woo, et al. [1] In their work the progress of two ligaments mechanical models were researched. The authors explained that the first quasi elastic model of ligament was implemented by Frisen. [6] The ligament model increased its stiffness gradually with increase of the load. A more advanced model was elaborated by Stuffier. [7] His model changed the patellar tendon with the kinematics chain composed of numbers of short

elements, pins, and torsion springs. Another model was used by Belkoff and Haunt. [8] The model assumed that the fibers were aligned in one direction. The model also postulated that the fibers were not straitened at the same time. The slack of each fiber was governed by the normal distribution function, $y(x) = Ae^{-Bx^2}$. The theoretical analysis for the equilibrium conditions of ligaments and tendons were conducted by Sidles, et al. [9] The authors confirmed that bending of the loaded fibers causes large transverse pressure and pressure gradients.

The main concern of the characterization of the mechanical behavior of ligaments and tendons, however, has been placed in the experimental approach. The results of the first experiment in this area were presented by Noyes [10], and Noyes and Grood. [11] The authors emphasized the aspects of the ligament stiffness, mechanical characteristics, and non-homogeneous material structure of human Anterior Cruciate ligament.

1.5 Need for Finite Element Analysis of ACL Prosthesis

The anterior cruciate ligament prosthesis has been thoroughly tested in many laboratories across the country and overseas. However, the prosthetic anterior cruciate ligament device that fulfills all the constrains that govern human knee has not been designed yet. The ACL is difficult to model due to dynamic mechanical properties and simulate the biological environment and conditions.

There are several problems associated with ACL prosthesis. The strength at the bone and ligament fixation is usually weak, bellows 50% the prosthetic material strength. Bone and ligament material interaction leads to a decrease in ultimate tensile strength of the device for over 50%. Poor ingrowth of bone cells in between ligament fibers cannot

stabilize prosthetic device in tibial as well as in the femoral tunnels. Non stabilized prosthetic devices experience excessive wear in tibial and femoral tunnels, and they are subjected to premature failure. Moreover, it has not been proven that tissue ingrowth increases ultimate tensile strength of the ligament prosthesis.

Consequently, there is a need for extensive biomechanical study of anterior cruciate ligament prosthetic device. Also, a detailed understanding of the stress distribution in the prosthetic ACL during various loading conditions is needed. The full Finite Element Analysis of the prosthetic ligament, tibia and femur bones, and screws bone fixation will provide answers to some difficult questions. For example, (1) how to locate and orient femoral and tibial tunnels to minimize bone ligament stress concentration. Thus, lower the wearing problem between prosthetic ACL, femur, and tibia. (2) How to design a prosthetic ligament to reduce its high stiffness and allow full range of knee joint motion.

1.6 Specific Objectives

The overall goal of this study was to develop a Finite Element Model of a prosthetic ligament yarn. The specific objectives of presented investigation were:

1) To develop a finite element model (FEM) of an artificial ligament yarn. The emphasis was put on the development of an elastic FEM.
2) To compare truss and beam element used in FEM to model yarn filaments. For example, to study the increase of stress due to a bending and twisting moment.
3) To find an optimum size for truss elements used in the finite element analysis (convergence study).

4) To analyze stress distribution in the ligament yarn filaments due to various loading conditions.

5) To analyze stress distribution in the ligament yarn filament due to change in yarn twisting length.

6) To compare results obtained from the Finite Element Analysis (FEA) of the ligament yarn model and the laboratory tensile tests.

1.7 Significance

Due to lack of positive results in clinical and animal testing of ACL deficient knee and the hope that synthetic ACL prosthesis will provide functional stability as well as the durability of the knee joint lead designer or engineer to use the fundamental method of stress analysis in the ACL prosthesis. The information obtained from the finite element model of a total prosthetic ACL will benefit the engineer and clinician to modify an existing prosthetic design and verify surgical procedures that will optimize stress distribution in the femur, prosthetic ACL, and tibia complex.

CHAPTER 2

FINITE ELEMENT MODEL OF SYNTHETIC LIGAMENT FILAMENT

Although both truss and beam elements that simulate the ligament yarn filaments are used in the FEM, truss elements are used after comparison. The truss element consists of two nodes. Three displacement degrees of freedom are defined at each node. Beam element is also composed of two nodes. However, three rotational degrees of freedom along with the displacement are defined. It has been proven that the bending and twisting moments in beam model do not contribute (with technical adequacy) to the normal shear stresses. Thus, only truss elements are selected in the FEM.

2.1 Yarn Filaments Modeling

The artificial ligament used in the FEM consists of 48 yarns. Each yarn is composed of a set of about 211 filaments. One filament is modeled as a truss element. The filaments are locally parallel to each other. A ligament yarn is modeled as a set of parallel truss elements. The filaments are twisted about the yarn's symmetry ax for stress analysis.

The normal stress due to bending moment that acts in the filament cross section is very small, so that it can be neglected. This stress can be solved from the equations as follows:

$$\sigma_{uu}(w) = -\frac{M_v w}{I_v}, \sigma_{uu}(v) = -\frac{M_w v}{I_w}, \text{ and } \tau(r) = -\frac{M_0 r}{I_0}. \qquad (2.1.1)$$

Where:

$$r = \sqrt{v^2 + w^2}\,.$$

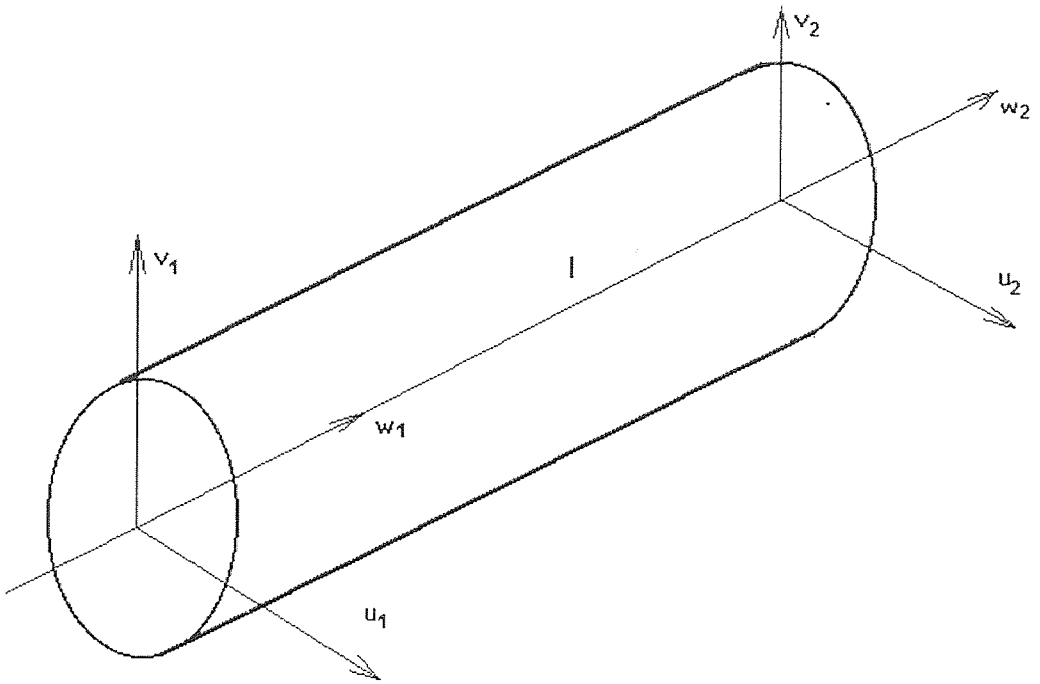

Figure 2.1.1 The truss element acted as a filament used in the FEM.

$$M_v = -EI_v\frac{d^2w}{du^2},\ M_w = -EI_w\frac{d^2v}{du^2},\ M_0 = -GI_0\frac{d\theta}{du}. \tag{2.1.2}$$

Therefore:

$$\sigma_{uu}(v) = -E\frac{d^2w}{du^2}v,\ \sigma_{uu}(w) = -E\frac{d^2v}{du^2}w,\ and\ \tau(r) = -G\frac{d\theta}{du}r. \tag{2.1.3}$$

The maximum stress on the filament cross section can be calculated from the following equations also.

$$\sigma_n = E\,\kappa\,R_f\ \ and\ \ \tau = G\frac{d\theta}{du}R_f \tag{2.1.4}$$

Where:

κ - filament curvature,

R_f - filament radius,

E - Young modulus,

G - Kirchoff constant,

θ - internal filament rotation angle.

2.2 Geometrical Description of the Ligament Filament

To find out the curvature κ and the derivative $\frac{d\theta}{du}$, a parametric model of the filament of the ligament was built. In the global coordinate system, x, y, and z, the ligament filament forms a spiral that can be described as follows:

$$\left\{\begin{array}{l} x = r\cos(2\pi t), \\ y = r\sin(2\pi t), \quad t = 0 \text{ to } 1 \\ z = l\,t \end{array}\right\} \tag{2.2.1}$$

Where:

r - distance between yarn's and filament's symmetry axis,

l - filament twisting length,

t - twisting control limit has a value from 0 to 1.

Or

$$r(t) = < r\cos(2\pi t),\ r\sin(2\pi t),\ lt >. \tag{2.2.2}$$

To calculate the curvature of the ligament filament, the first and the second derivative of this location vector of x, y, and z (equation 2.2.1) is needed. The curvature is calculated from the following equation:

$$\kappa = \frac{\left| r'(t) \times r''(t) \right|}{\left| r'(t) \right|^3} \tag{2.2.3}$$

So

$$r'(t) = < -2\pi r \sin(2\pi t),\ 2\pi r \cos(2\pi t),\ l > \tag{2.2.4}$$

$$\left| r'(t) \right| = \sqrt{4\pi^2 r^2 + l^2}\ , \tag{2.2.5}$$

$$r''(t) = < -4\pi^2 r \cos(2\pi t),\ -4\pi^2 r \sin(2\pi t),\ 0 > \tag{2.2.6}$$

$$r'(t) \times r''(t) = \begin{vmatrix} i, & j, & k, \\ -2\pi r \sin(2\pi t), & 2\pi r \cos(2\pi t), & 1 \\ -4\pi^2 r \cos(2\pi t), & -4\pi^2 r \sin(2\pi t), & 0 \end{vmatrix} \tag{2.2.7}$$

$$= 4\pi^2 r < l \sin(2\pi t),\ -l \cos(2\pi t),\ 2\pi r >$$

Therefore:

$$\left| r'(t) \times r''(t) \right| = 4\pi^2 r \sqrt{4\pi^2 r^2 + l^2}\ . \tag{2.2.8}$$

Finally:

$$\kappa = \frac{\left| r'(t) \times r''(t) \right|}{\left| r'(t) \right|^3} = \frac{4\pi^2 r \sqrt{4\pi^2 r^2 + l^2}}{\left(\sqrt{4\pi^2 r^2 + l^2} \right)^3} = \frac{4\pi^2 r}{4\pi^2 r^2 + l^2}\ . \tag{2.2.9}$$

If the internal twisting is linear over the filament length l, the $\frac{d\theta}{du}$ can be calculated from the following equation:

$$\frac{d\theta}{du} = \frac{2\pi}{s}\ . \tag{2.2.10}$$

Where:

s - arc length,

$$s = \int_0^1 \sqrt{\left(x'(t)\right)^2 + \left(y'(t)\right)^2 + \left(z'(t)\right)^2}\ dt = \int_0^1 \left| r'(t) \right| dt. \tag{2.2.11}$$

So:

$$s = \sqrt{4\pi^2 r^2 + l^2}\,. \tag{2.2.12}$$

And:

$$\frac{d\theta}{du} = \frac{2\pi}{\sqrt{4\pi^2 r^2 + l^2}}\,. \tag{2.2.13}$$

2.3 Approximation of the Stress from Bending and Twisting of the Ligament Filament

The maximum stress exerted on the filament due to bending and twisting can be presented in an equation form. From equations 2.1.4 and 2.2.9, the normal stress on the filament has the following form:

$$\sigma_n = E\,\kappa\,R_f = E\,R_f\,\frac{4\pi^2 r}{4\pi^2 r^2 + l^2}\,. \tag{2.3.1}$$

The shear stress is calculated using equation 2.1.4 and 2.2.13.

$$\tau = G\,\frac{d\theta}{du}\,R_f = G\,R_f\,\frac{2\pi}{\sqrt{4\pi^2 r^2 + l^2}}\,. \tag{2.3.2}$$

Where:

- E - Young modulus,
- G - Kirchoff constant,
- R_f - filament radius,
- l - section length.

2.4 Average Radius of the Yarn of a Ligament

Line segments that connect filament centers are modeled as contact elements. Each filament occupied an area that is approximately equal to the area of hexagon that overlaps the filament (Figure 2.4.1). The following equation describes the appropriate relationship:

$$A_f = 6\, R_f \frac{R_f\sqrt{3}}{3} = 2\, R_f^2\sqrt{3}. \qquad (2.4.1)$$

The total area that is occupied by the yarn is proportional to the number of filaments and the area of each filament. Therefore:

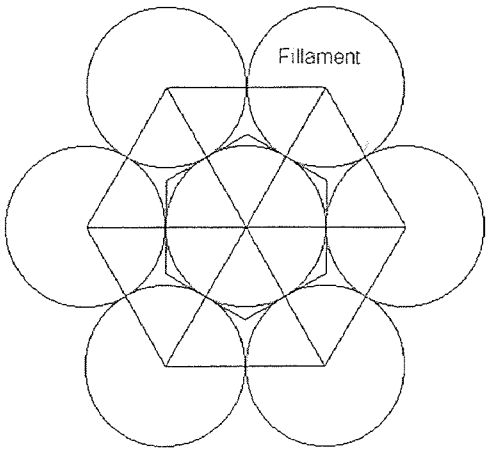

Figure 2.4.1 A cross section of yarn that builds from seven filaments

$$A_t = 2\, nR_f^2\sqrt{3}. \qquad (2.4.2)$$

On the other hand, the average area of the ligament yarn is estimated from the following equation:

$$A_t = \pi R_t^2. \qquad (2.4.3)$$

Finally, the equation of the average yarn size is:

$$R_t = R_f\sqrt{\frac{2n\sqrt{3}}{\pi}}. \qquad (2.4.4)$$

Where:

A_f - filament area,

A_t - yarn area,

n - number of filaments in the yarn,

R_f - filament radius,

R_t - average yarn radius,

$\pi = 3.1415926...$

2.5 Numerical Values of Normal and Shear Stress Compared to the Normal Tensile Stress due to Bending and Twisting Forces Along the Yarn Radius

2.5.1 Residual Stresses

The yarn is composed of 211 filaments. The radius of each filament R_f is approximately equal to 9.735[μm] and the twisting length l is equal to 2500[μm]. In addition, E is assumed to be 14.5[GPa] which was obtained from the experimental testing use Dacron® (Table 3.4.1b). The average yarn radius is calculated from 2.4.4 equation,

$$R_t = R_f\sqrt{\frac{2n\sqrt{3}}{\pi}} = 148.5\mu m \tag{2.5.1}$$

The maximum normal stress on the filament due to bending moment is calculated from equation 2.3.1.

$$\sigma_n = E\,R_f\,\frac{4\pi^2 r}{4\pi^2 r^2 + l^2}. \tag{2.5.2}$$

The results of σ_n are summarized in graph (Figure 2.5.1) with the assumption that ν = 0.3

$$G = \frac{E}{2\left(1+\nu\right)}. \tag{2.5.3}$$

The shear stress can be calculated from equation 2.3.2.

$$\tau = \frac{\pi R_f E}{\left(1+\nu\right)\sqrt{4\pi^2 r^2 + l^2}}. \tag{2.5.4}$$

2.5.2 Normal and Shear Stress Due to a Change in Filament Curvature

During the elongation of the yarn, not only the curvature of filament changes so as the normal stress (Figure 2.5.1). The assumption for this calculation is that the filament cross sections are infinitely stiff.

$$\Delta\sigma_n = 4\pi^2 r\, E\, R_f \left(\frac{1}{4\pi^2 r^2 + l_2^2} - \frac{1}{4\pi^2 r^2 + l_1^2} \right). \qquad (2.5.5)$$

Where:

l_1 - initial filament section length,

l_2 - final filament section length.

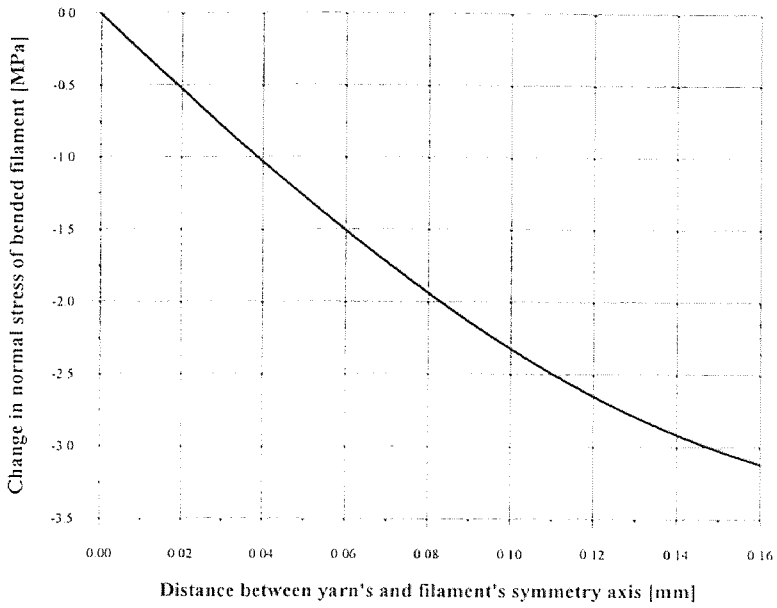

Figure 2.5.1 Change in the normal stress due to the change of the filament curvature. Elongation equal to 1.5% of its initial length.

An increase of normal stresses due to the change of filament Figure 2.5.1. An 1.5% increase of initial filament length for the total elongation is assumed. The initial length l_1 is equal 2.5 [mm].

The change in shear is calculated from the following equation:

$$\Delta\tau = \frac{\pi R_f E}{1+\nu}\left(\frac{1}{\sqrt{4\pi^2 r^2 + l_2^2}} - \frac{1}{\sqrt{4\pi^2 r^2 + l_1^2}}\right). \tag{2.5.6}$$

and displayed in figure 2.5.2.

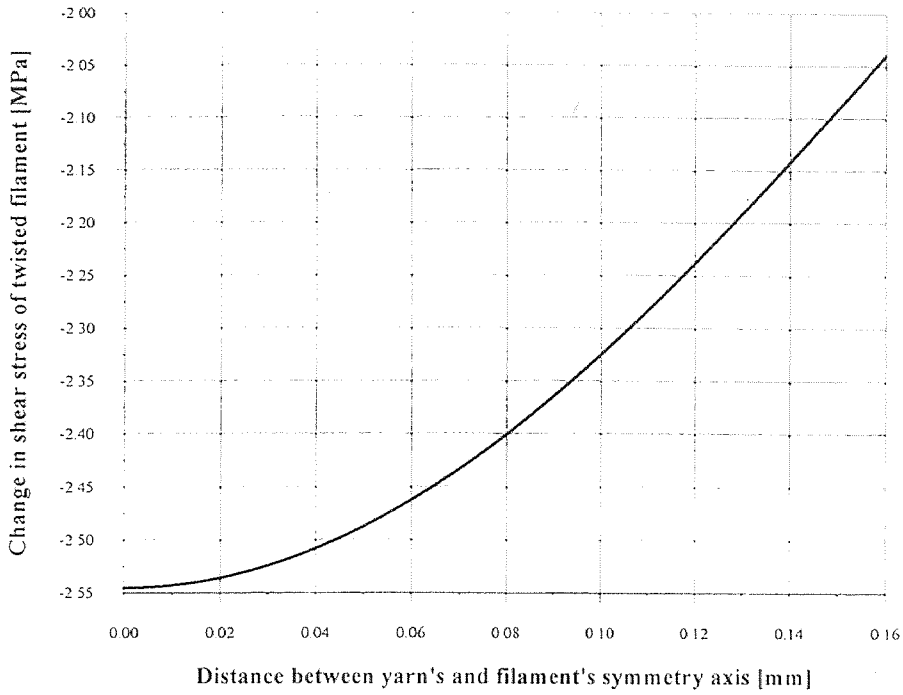

Figure 2.5.2 Change in the shear stress in the filament due to the curvature change during elongation.

2.5.3 Maximum Normal Stress Due to Yarn Elongation

The yield force F_t acting on the yarn is not greater than 10N. Therefore, in the axial or longitudinal loading condition, the normal stress on filament cross section is less than:

$$\sigma_{n,\,tensile} < \frac{F_t}{n\pi R_f^2} = 179\ [MPa]. \tag{2.5.7}$$

CHAPTER 3

FILAMENT TO FILAMENT INTERFACE MODELING

Although it is difficult to expect any big variations in filament interconnecting stress along the filaments, the truss element can be used as a sufficient tool in the model. The filament to filament interconnecting stresses was determined truss discreet and the total energy equivalence.

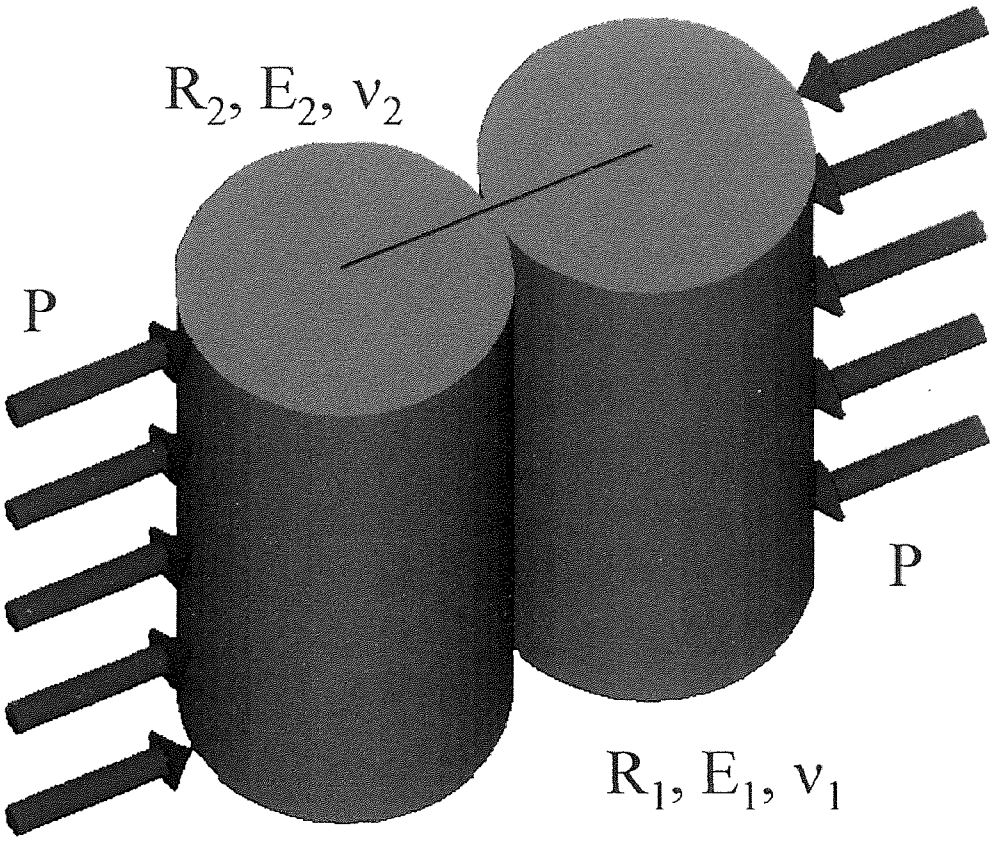

Figure 3.1.1 Filament to filament contact stress.

3.1 The Stiffness of Interconnecting Element - Hertzian Theory

The contact stresses must be taken in to a consideration during the investigation since filaments are only contacted on the surface and they cannot interact internaly with each other. The inter-filament stiffness is calculated based on Hertzian Theory. [12] The radius of contact surface area, b, is given by:

$$b = 1.13\sqrt{P\frac{R_1R_2}{R_1 + R_2}\left(\frac{1-\nu_1^2}{E_1} + \frac{1-\nu_2^2}{E_2}\right)} \tag{3.1.1}$$

The maximum stress between two cylinders in contact is given from the equation:

$$\sigma_{max} = 0.564\sqrt{P\left(\frac{1}{R_1} + \frac{1}{R_2}\right)\left(\frac{1-\nu_1^2}{E_1} + \frac{1-\nu_2^2}{E_2}\right)^{-1}} \tag{3.1.2}$$

Where:

R_1, R_2 - cylinder radius,

E_1, E_2 - Young modulus for first and second cylinders respectively,

ν_1, ν_2 - Poisson's ratio,

P - contact pressure,

b - contact area radius,

σ_{max} - maximum contact stress.

In the present analysis, it is assumed that:

$$E_1 = E_2 = E,\ \nu_1 = \nu_2 = \nu, \text{ and } R_1 = R_2 = R_f. \tag{3.1.3}$$

Therefore, equation 4.1.1, and 4.1.2 becomes:

$$b = \sqrt{\frac{4}{\pi}PR_f\left(\frac{1-\nu^2}{E}\right)}, \tag{3.1.4}$$

$$\sigma_{max} = 0.564\sqrt{\frac{P}{R_f}\left(\frac{E}{1-\nu^2}\right)}. \tag{3.1.5}$$

The strain can be calculated from equation:

$$\varepsilon = \frac{\Delta R_f}{R_f} = 1 - \sqrt{1 - \frac{4}{\pi}\frac{P}{R_f}\left(\frac{1-\nu^2}{E}\right)}\,. \tag{3.1.6}$$

Finally, the stiffness per unit length is defined in the following equation:

$$\eta = \frac{\Delta P}{\Delta \varepsilon} = \frac{P}{1 - \sqrt{1 - \frac{4}{\pi}\frac{P}{R_f}\left(\frac{1-\nu^2}{E}\right)}}\,. \tag{3.1.7}$$

3.2 Estimation of Filament's Interconnection Stiffness for the Finite Element Model

To calculate the stiffness of interconnecting elements in building the FEA model, maximum pressure that is perpendicular to the ligament filament surface should be estimated (Figure 3.2.1).

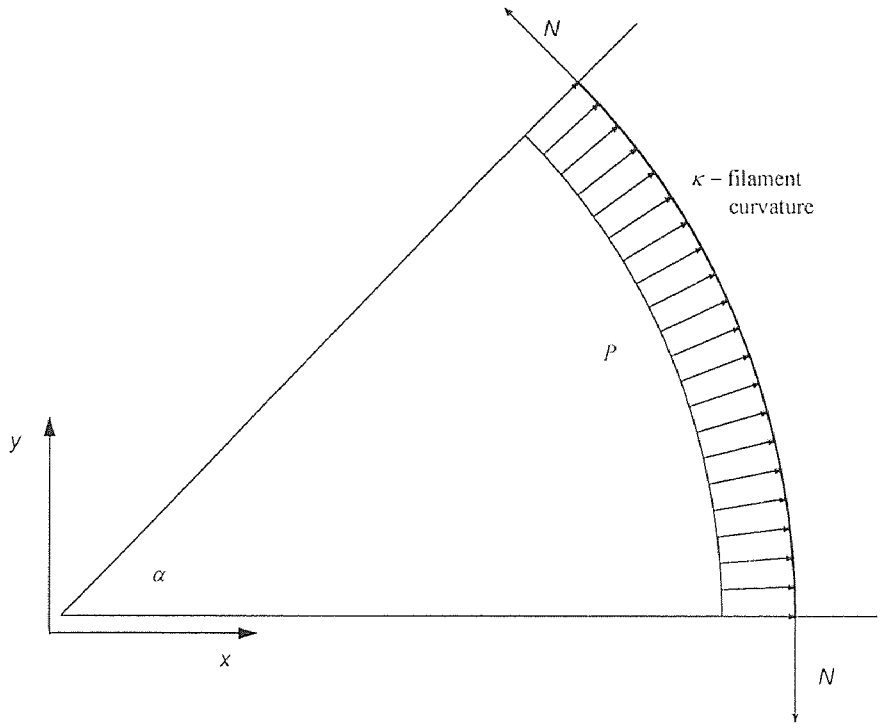

Figure 3.2.1 Forces that act on the filament with known curvature.

The filament shown in Figure 3.2.1 is in a static equilibrium condition. That is the sum of all forces and the moment acting on it are equal to zero. Therefore, the sum of x components of all forces must equal zero.

$$\int_0^{\alpha} \left(\frac{P}{\kappa}\right) \cos(\beta) d\beta + N \cos(\frac{\pi}{2} + \alpha) = 0, \tag{3.2.1}$$

$$\frac{P}{\kappa} \sin(\beta)\Big|_0^{\alpha} + N \cos(\frac{\pi}{2} + \alpha) = 0, \tag{3.2.2}$$

$$\frac{P}{\kappa} \sin(\alpha) - N \sin(\alpha) = 0. \tag{3.2.3}$$

Finally,

$$\frac{P}{\kappa} - N = 0 \quad \text{or} \quad P = \kappa N. \tag{3.2.4}$$

The sum of all y force components is also equal to zero. By using κ from the equation 2.2.9, the side pressure on the filament is calculated as follows.

$$P = N \frac{4\pi^2 r}{4\pi^2 r^2 + l^2}. \tag{3.2.5}$$

3.3 First Order Approximation of the Interconnecting Element Stiffness for the Finite Element Modeling

To find more accurate stiffness of interconnecting elements, following calculations and assumptions are made. First, it is assumed that the n is the total number of filaments in the ligament yarn. F is the total external force imposed on the yarn and it is distributed equally in each filament. The filament tension N due to the external load is defined from the equation 3.2.1. The most loaded filaments are lying on the external radius of the yarn. These assumptions will be verified with FEM solutions (see section 6.3.1). Next, in the numerical calculation (used as an example), the total force F exerted on the yarn is 10[N].

The total number of filaments, n, in the yarn is equal to 211. The ligament yarn length l is equal to 2.5 [mm] (360^0 twisting length). So,

$$N = \frac{F}{n} = 47.4\,[mN], \tag{3.3.1}$$

If the yarn external radius $r = 0.16$ [mm], the side pressure on the filament is calculated from equation 3.2.5:

$$P = N\frac{4\pi^2 r}{4\pi^2 r^2 + l^2} = 41.2\left[\frac{mN}{mm}\right]. \tag{3.3.2}$$

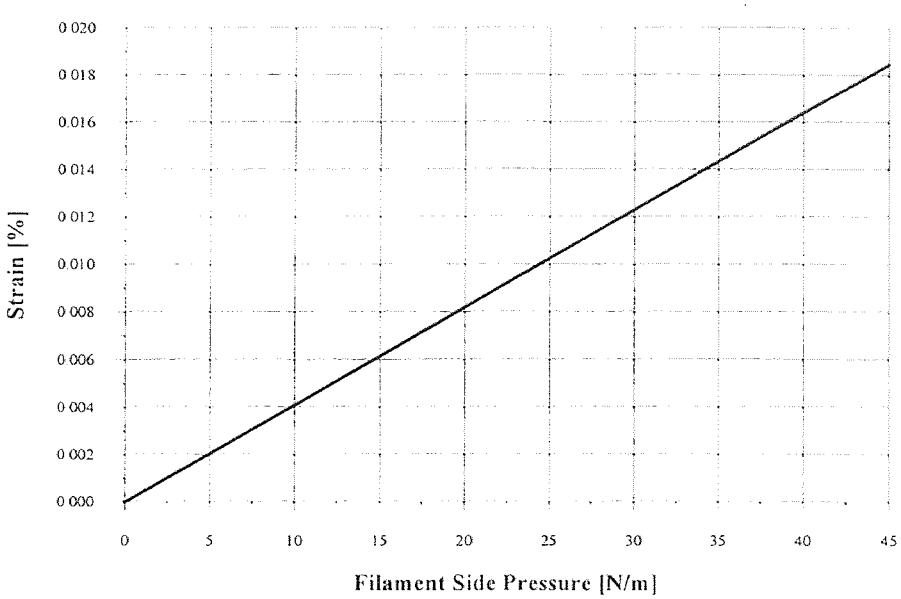

Figure 3.3.1 Filament side strain as a function of side pressure. Equation 3.1.6 for pressure side range calculated above.

It is not difficult to notice that the strain versus side pressure curve is linear over the expected range of the pressure. Therefore, the stiffness of the filament, η can be calculated from the linear approximation.

$$\eta = \frac{\Delta P}{\Delta \varepsilon} = 243.66\,\left[\frac{N}{mm}\right] \tag{3.3.3}$$

3.4 Finite Element Model Coordinate System

The coordinates of each node are circumscribed in rectangular global coordinate system. However, a nodal coordinate system is also defined for each node. The z axis of a node is parallel to the Z axis of the global coordinate system. The x and y are parallel to the radial and circumferential directions of the global cylindrical coordinate system (Figure 3.4.1).

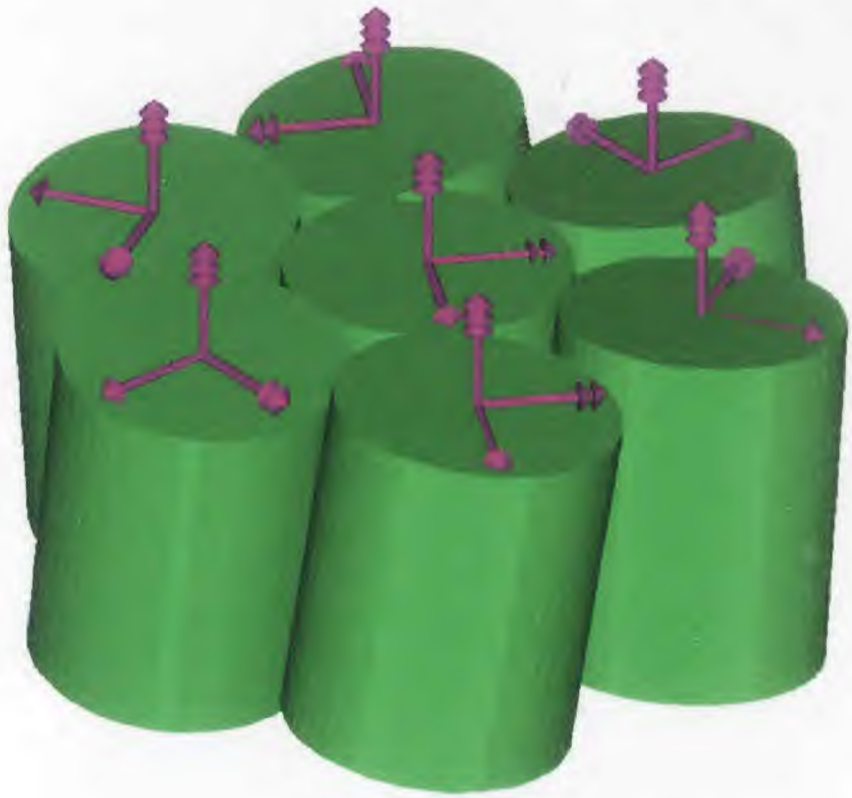

Figure 3.4.1 Nodal coordinate system definition. Each node is defined in its coordinate systems. Single, double, and triple arrow represents x, y, and z local coordinate, respectively.

Although the yarn geometry is naturally described in cylindrical coordinate system, the rectangular coordinate system was used. Although the geometrical properties of the yarn has a screwlike symmetry, the cylindrical coordinate system was not selected since

this coordinate system is not properly handled in the Ansys 5.0, FEM program. However, the cyclindrical coordinated system was used to generate yarn model which is used in the calculations.

3.5 Boundary Condition

Due to the capatibility of translation and rotation mechanizm of the yarn, it can be modeled with in infinitely small segment (all cross section will provide the same information). However, for the purpose of finite element modeling, finite length of filament elements are used. All nodes are constrained in circumferential direction due to cylindrical symmetry. Nodes with X=0, Y=0, and Z=0 has no displacement. All nodes with Z=0 have no Z displacement. Displacement of all nodes with Z=l are proportional to the yarn strain and length (Figure 3.5.1).

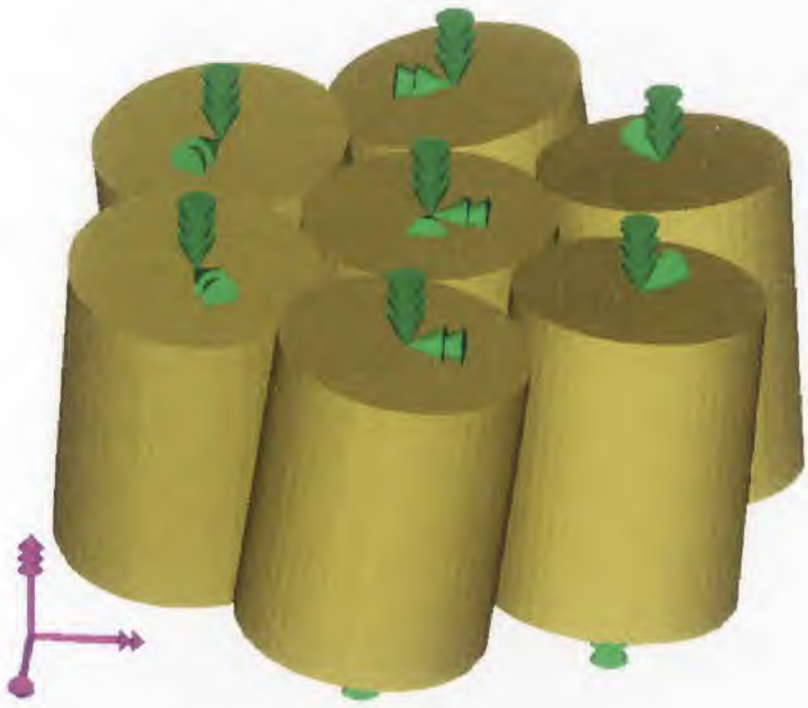

Figure 3.5.1 Boundary condition.

CHAPTER 4

RESULTS FROM FINITE ELEMENT ANALYSIS

4.1 Convergence Study

For the purpose of convergence study, several calculations of total force on the yarn for 1.5% strain are made. In this study, it is assumed that only the lengths of longitudinal elements are changed.

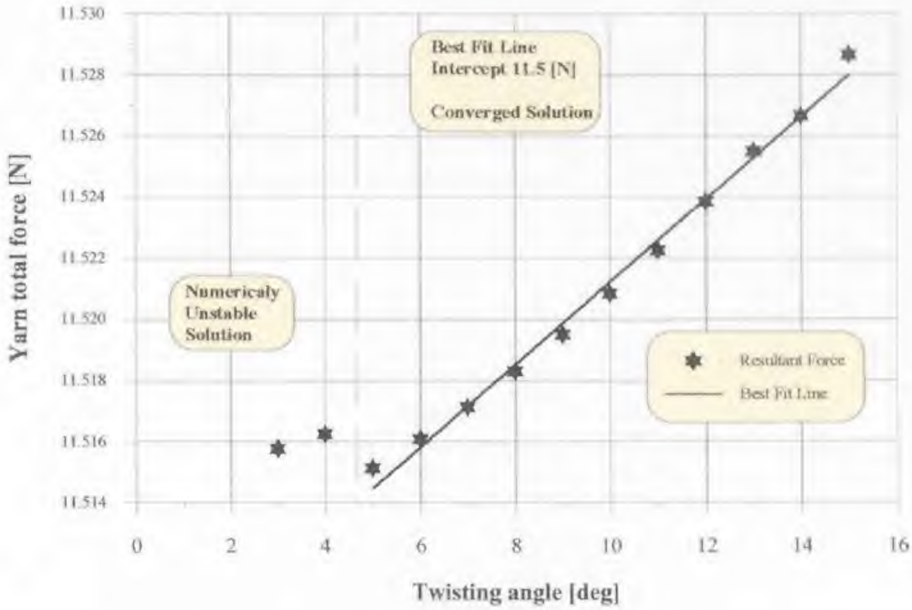

Figure 4.1.1 Sum of all components of all forces that are parallel to the yarn axis of symmetry.

The lengths of element are proportional to the yarn twisting length and the angle between the cross section planes, element twisting angle. This angle is used as a parameter of the study.

$$l_e = \sqrt{4r^2 \sin^2\left(\frac{\theta_f}{2}\right) + \left(\frac{\theta_f}{2\pi}\right)^2 l^2} \qquad (4.1.1)$$

Where:

θ_f - element twisting angle,

r - distance between yarn's and filament's symmetry axis,

l_e - element length,

l - twisting length.

Element twisting angle is proportional to the final element's length. The lower the element twisting angle, the smaller the element size. Figure 4.1.1 shows that the smaller the longitudinal elements, the solution converged, but only up to 5^o of twisting angle. This fact is due the finite representation of real numbers in computer's memory.

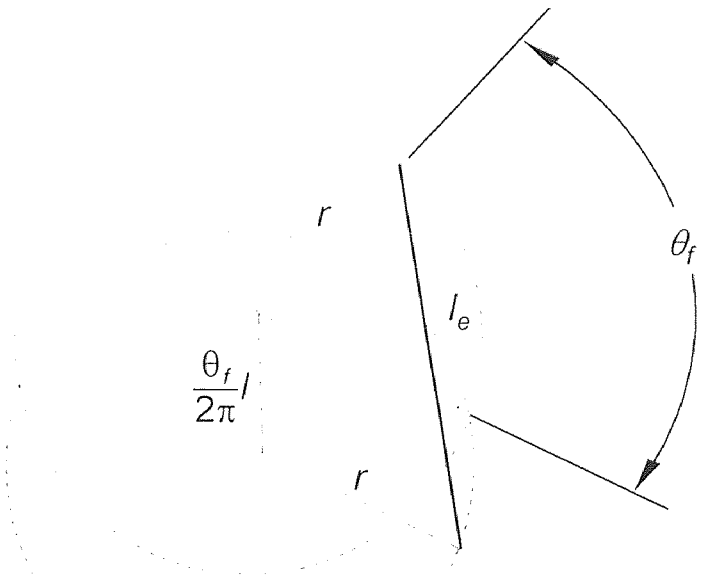

Figure 4.1.2 Element twisting angle definition.

The filament internal forces and stresses are collected in Figures 4.1.3 and 4.1.4. The contact forces and stresses are collected in Figures 4.1.5 and 4.1.6.

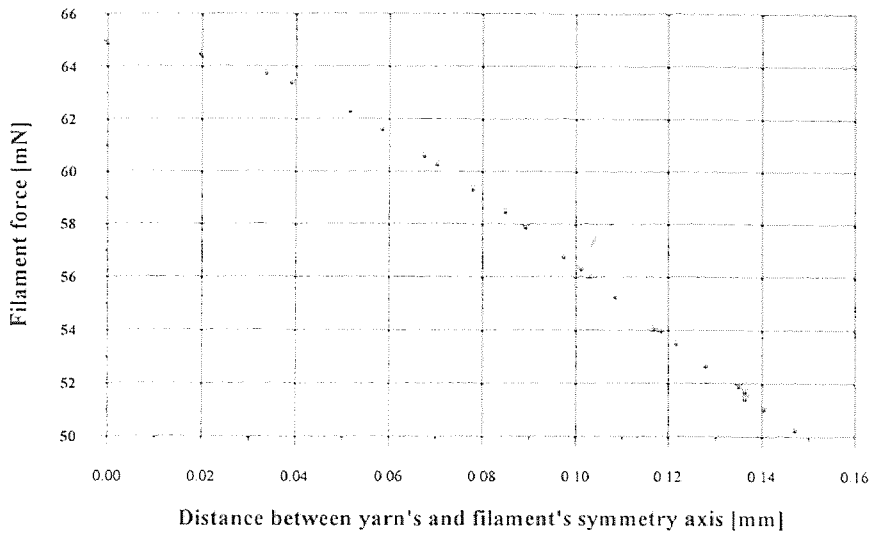

Figure 4.1.3 Filament normal force with respect to its cross section as a function of the distance between yarn's and filament's symmetry axis.

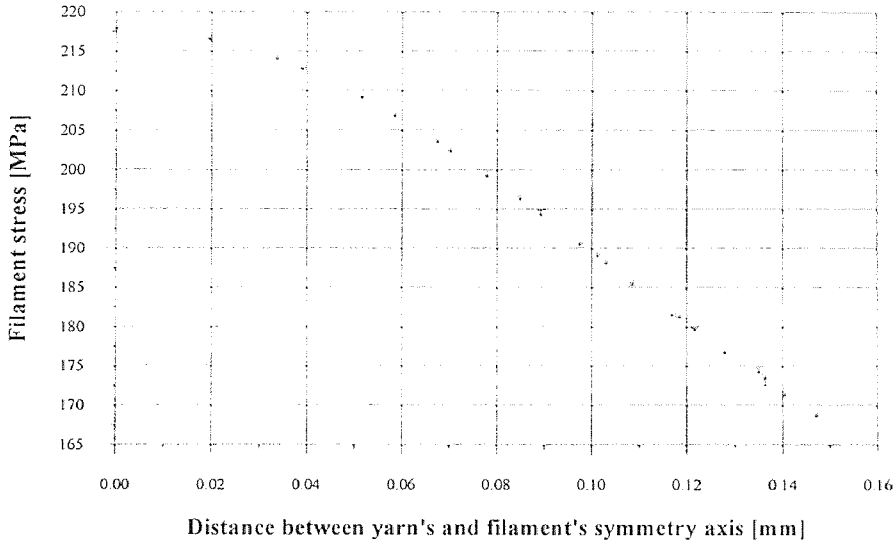

Figure 4.1.4 Filament normal stress with respect to its cross section as a function of the distance between yarn's and filament's symmetry axis.

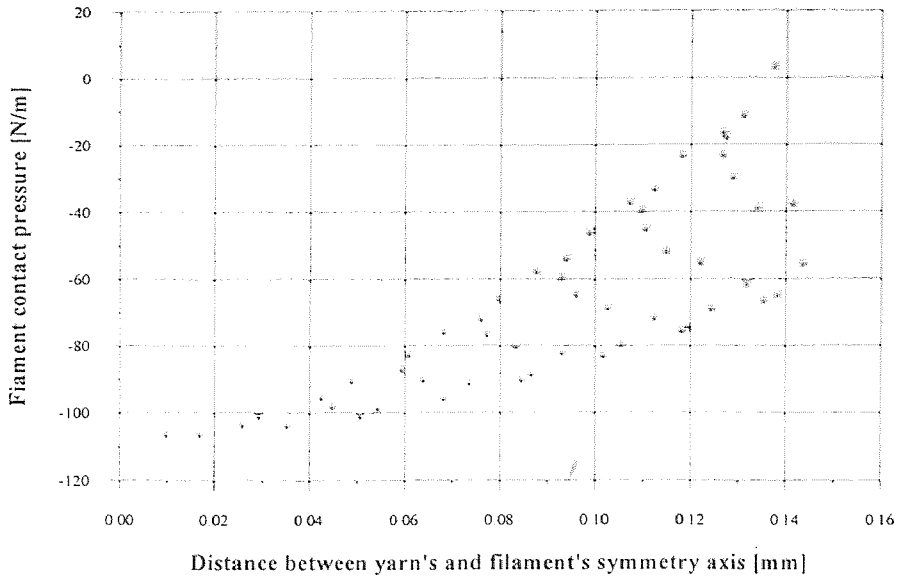

Figure 4.1.5 Filament to filament contact pressure, normal to the interface plane with respect to its cross section as a function of the distance between yarn's and filament's symmetry axis.

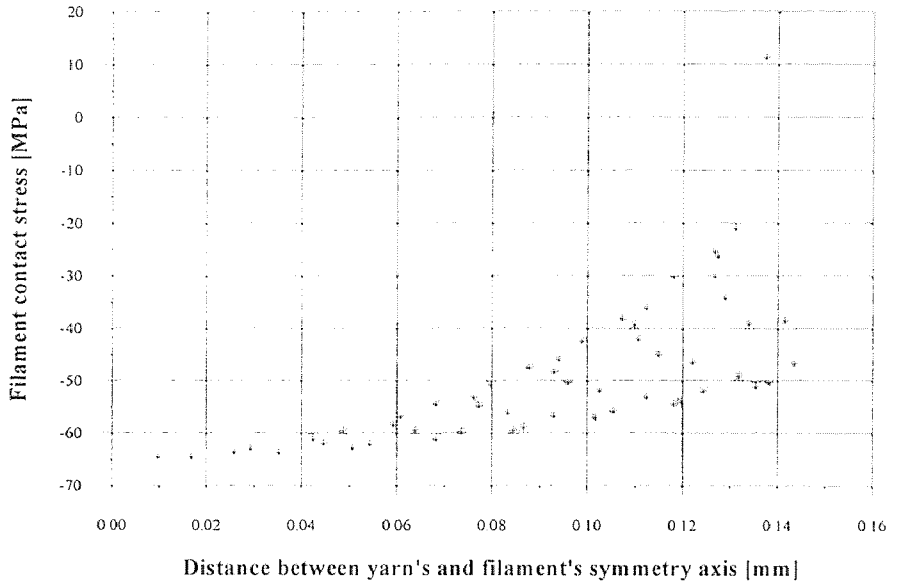

Figure 4.1.6 Filament to filament contact stress with respect to its cross section as a function of the distance between yarn's and filament's symmetry axis.

It can be noticed that the contact stresses and pressures have positive values at one point. Although stretching the filament instead of squeezing occurred in this case, most of the contact elements work in the proper direction.

4.2 Yarn Internal Forces as a Function of Strain

The filament force and stress are calculated as a function of total strain. Four levels of strain are chosen, 0.375, 0.75, 1.125 and 1.5% of the total yarn length. The results of finite element calculation are displayed in the following graphical form. Stress strain curve is shown in Figure 4.2.1. Filament normal forces and stresses are presented in Figures 4.2.2 and 4.2.3. Filament contact pressure and stress are given in Figures 4.2.4 and 4.2.5.

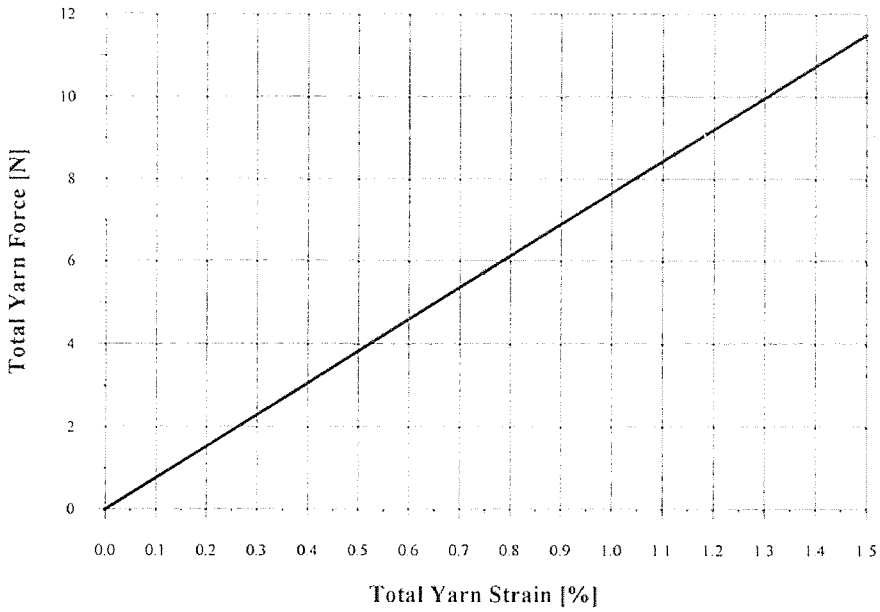

Figure 4.2.1 Total yarn force as a function of yarn strain.
All calculations are made with 2.5 mm yarn twisting length.

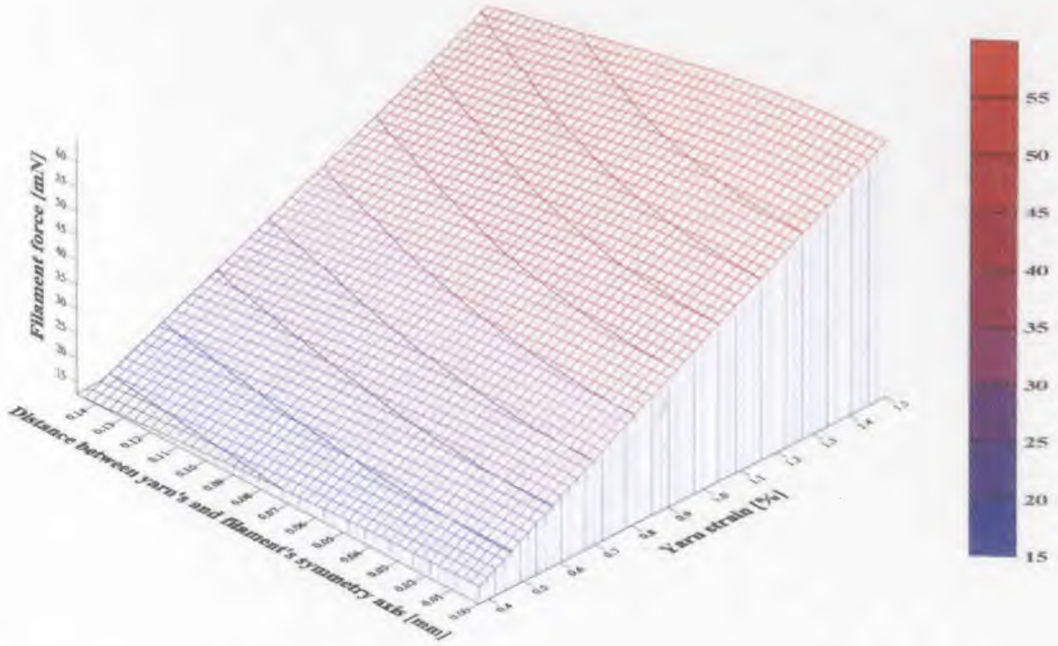

Figure 4.2.2 The distribution of filament force at four strains levels.

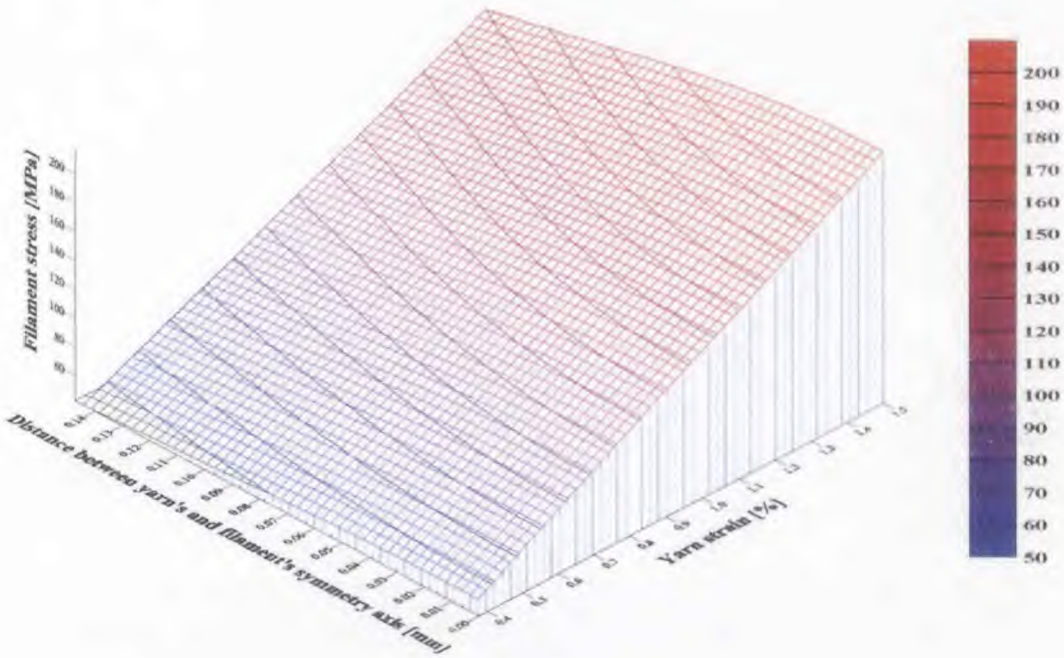

Figure 4.2.3 The distribution of filament stress as a function of yarn strain.

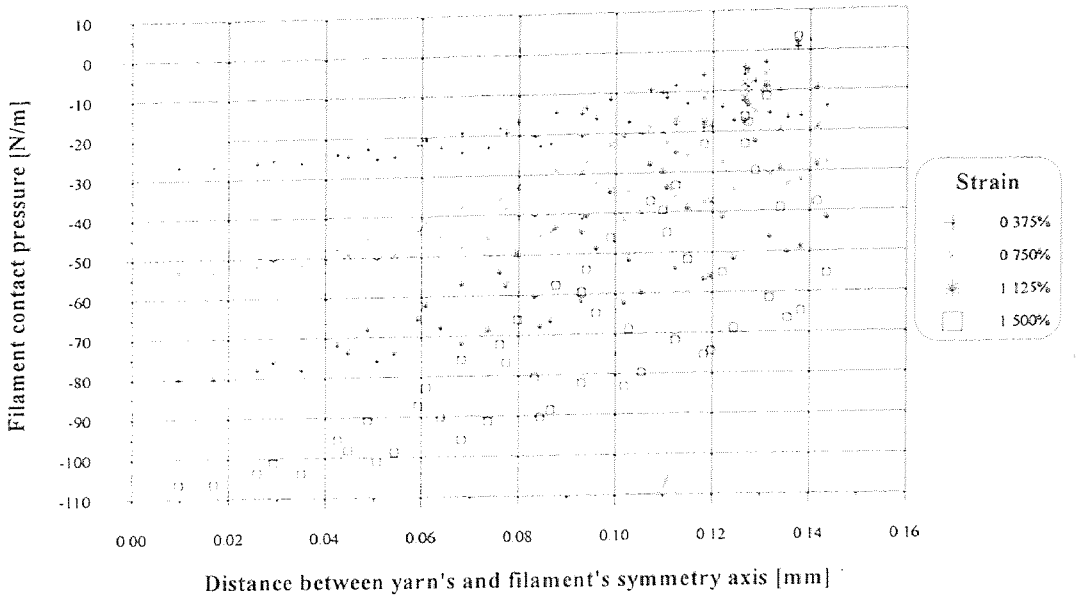

Figure 4.2.4 The filament contact pressure distribution as a function of yarn strain.

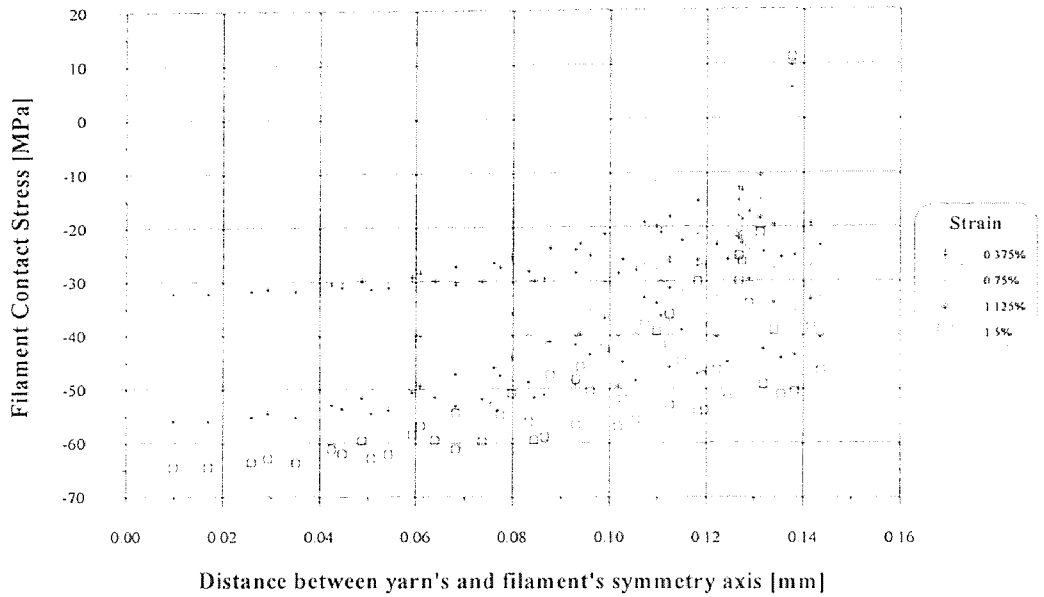

Figure 4.2.5 Maximum filament contact stress as a function of total yarn strain.

The data presented above describes that the major portion of the stress is carried by the filaments that is located on the yarn symmetry axis. The filament also carries the most

contact and normal load. It can be concluded that this filament is going to fail at first during loading. The finite element solution shows that stress strain curve is linear (Figure 4.2.1) since a linear, an isotropic, and a homogeneous material property of the yarn was assumed in the modeling.

4.3 Optimization of Yarn Twisting Length

The changes in total yarn force, stresses, and total stiffness are all calculated as a function of its twisting length. All calculations are conducted under the same geometrical condition, material properties of filaments, boundary, and loading conditions as described in the previous sections. Eleven different twisting lengths are used during calculation. All results are based on 1.5% total yarn strain.

4.3.1 Results

Plots of the total force and resultant modulus of the yarn as a function of its twisting length is shown in Figures 4.3.1 and 4.3.2 respectively. Plots of the filament cross section normal force and stresses distribution with respect to the filament location in the yarn versus the yarn twisting length are summarized in Figures 4.3.3 and 4.3.4. Plots of the pressure and contact stress between filaments as a function of the yarn twisting length and filament location in the yarn are shown in Figures 4.3.5 and 4.3.6. Some data were excluded from Figures 4.3.5 and 4.3.6 for the clarity purpose.

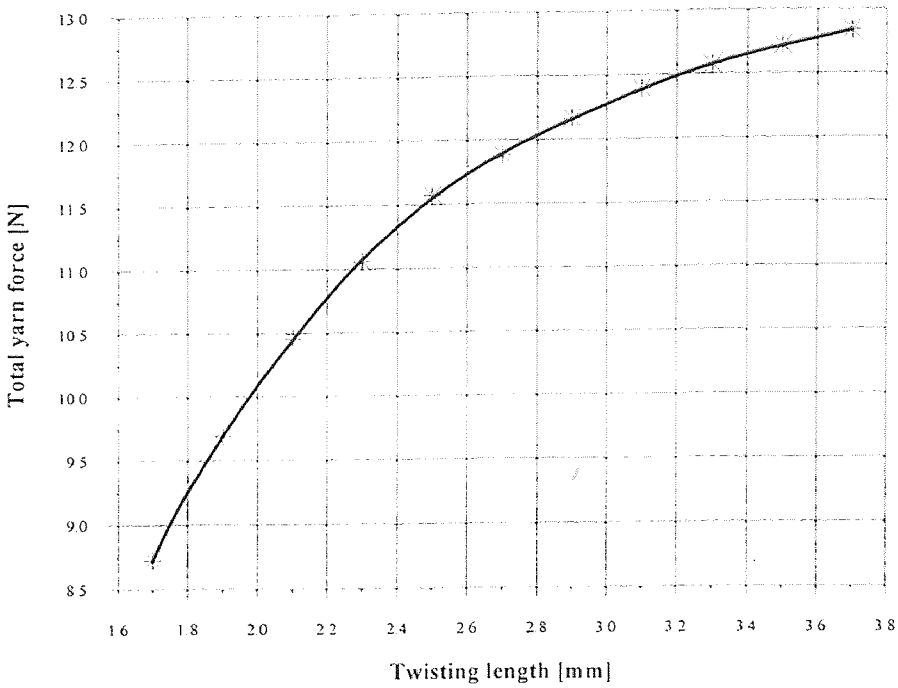

Figure 4.3.1 Total yarn force as function of its twisting length.

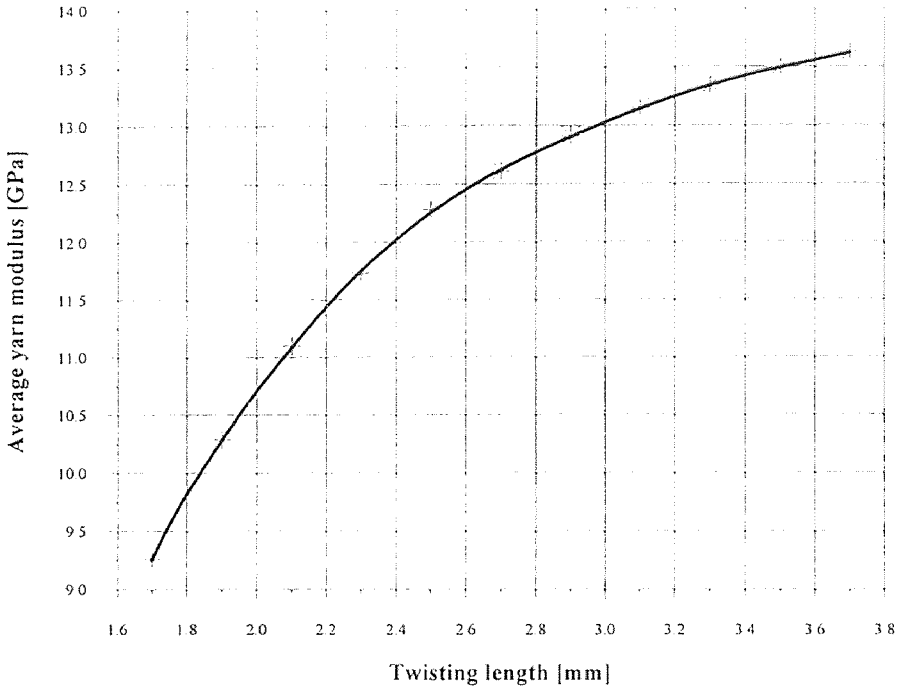

Figure 4.3.2 Average yarn modulus as a function of its twisting length.

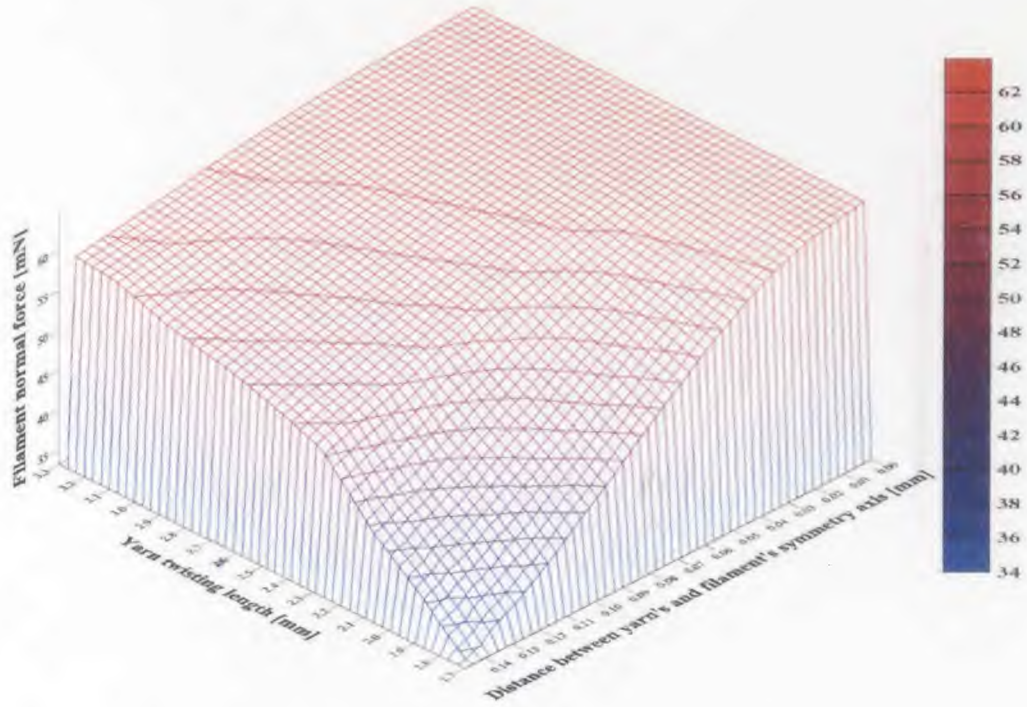

Figure 4.3.3 The distribution of filament force along yarn radius as a function of the twisting length of the yarn.

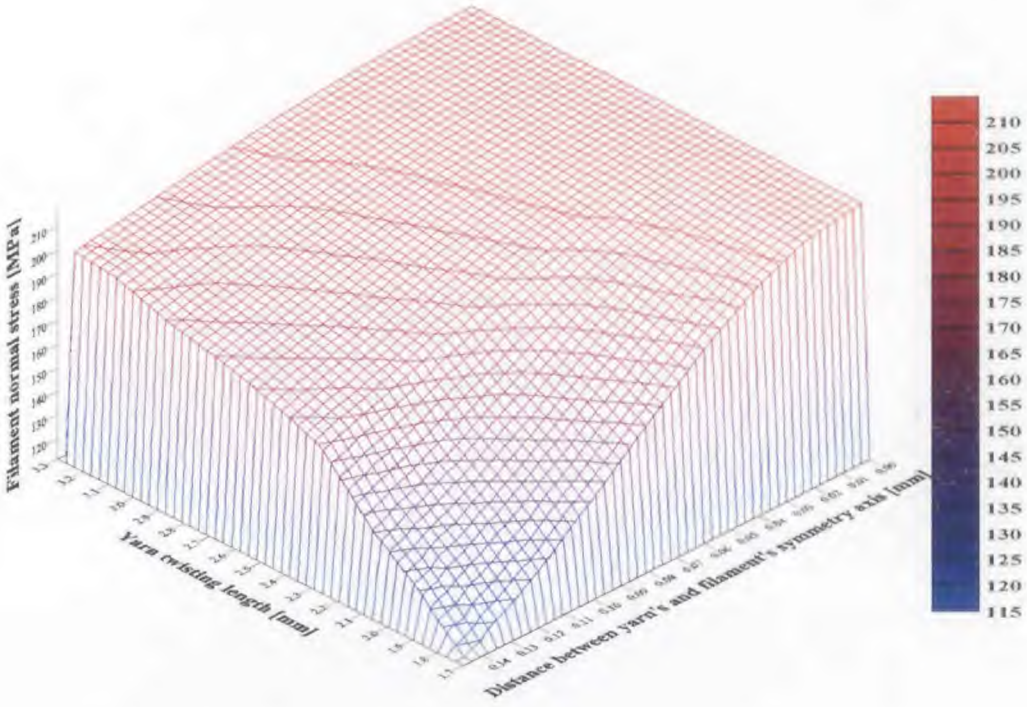

Figure 4.3.4 The distribution of filament stress along yarn radius as a function of the twisting length of the yarn.

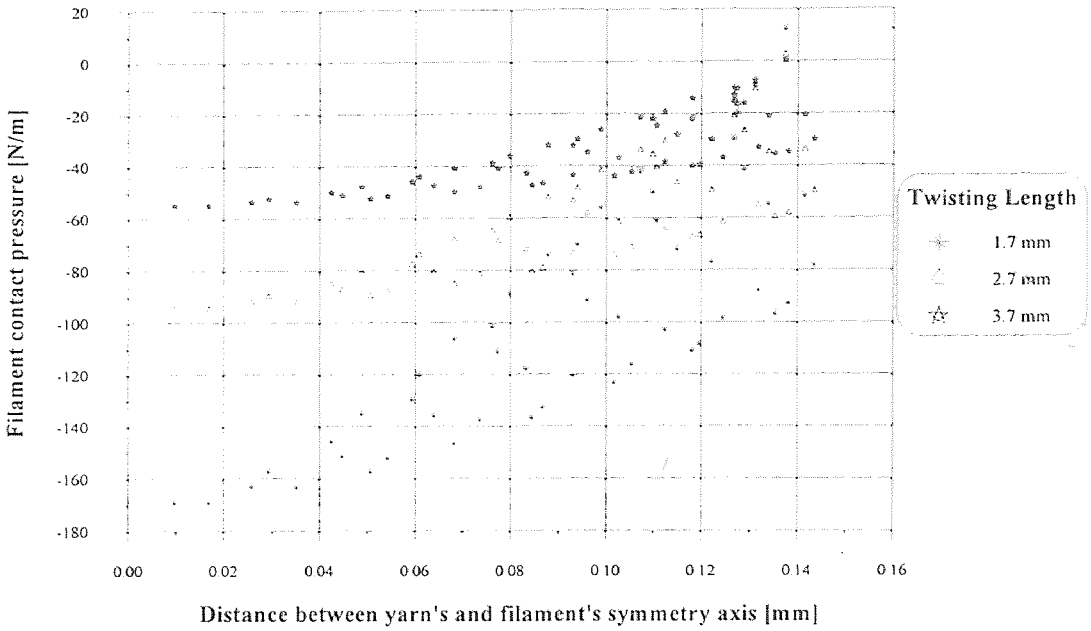

Figure 4.3.5 The distribution of filament contact pressure along yarn radius as a function of the twisting length of the yarn.

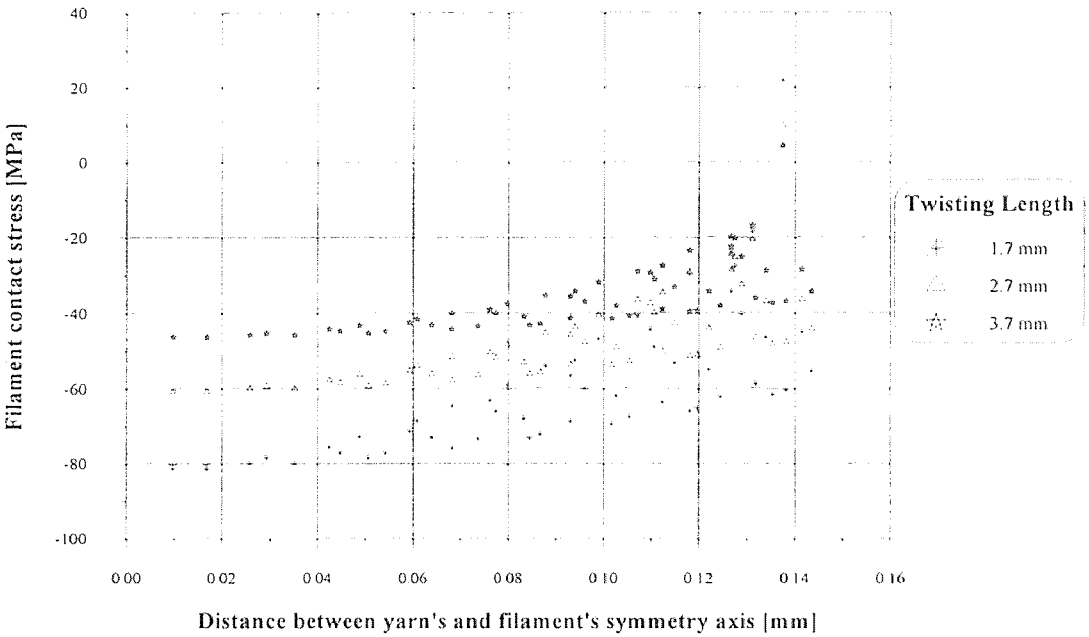

Figure 4.3.6 The distribution of filament maximum contact stress along yarn radius as a function of the twisting length of the yarn.

CHAPTER 5

EXPERIMENTAL FINDINGS

5.1 The Ultimate Tensile Stress of the Yarn

A simple tensile test of yarn was made for the purpose of determination of the change in the mechanical properties of Dacron™ yarns for the twisted and untwisted yarns.

5.1.1 Material and Method

Two types of designed Dacron™ yarn were tested. A single ply yarn and a twisted double plies yarns were received from DuPoint. Non-twisted yarn was consisted of 95 equal diameter filaments. The twisted yarn contained 190 filaments and it was twisted along the symmetry axis with 2.5 mm twisting length. Six Dacron™ yarns for each design type were tested in each experiment. The samples were prepared according to following procedure. The ends of each yarn were attached to a 1/8" of diameter and 1" long polyethylene rigid tube with a 1/4" long wood pin. The remaining tube space was filled with Devcon 5-minute epoxy (Figure 5.3.1). The samples were tested (tensile test) to break. The equipment used is the Chatillon Elongation Control Tensile Machine. Strain versus stress results were recorded by data acquisition system based on (COMPAQ computer) and Chatillon software.

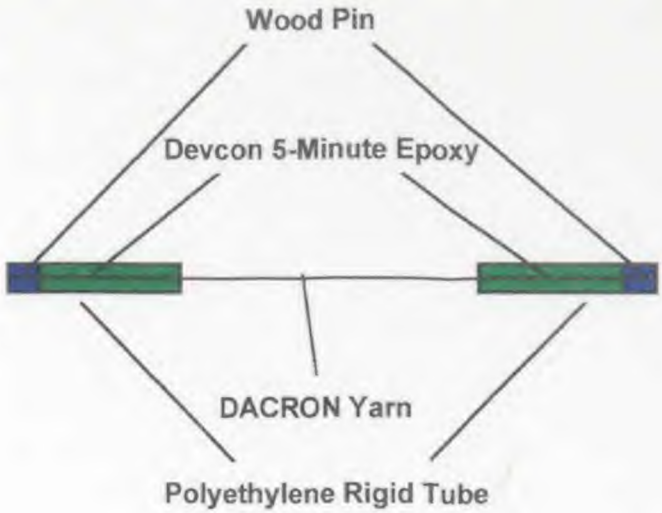

Figure 5.2.1 The setup of DACRON® yarn for the mechanical testing.

5.1.2 Results

Typical load-strain curves for twisted and not-twisted yarns are shown in Figures 5.3.1 and 5.3.2. The calculated results for the yield load, yield elongation, ultimate tensile strength, ultimate tensile elongation, stiffness, yield stress, yield strain, ultimate tensile stress, ultimate tensile strain, and modulus are shown in Tables 5.3.1a, 5.3.1b, 5.3.2a and 5.3.2b, respectively.

Table 5.3.1a Material properties of single ply, non-twisted Dacron™ yarn.

Sample Number	Gage Length (mm)	Yield Load (N)	Yield Elongation (mm)	Max. Load (N)	Max. Elongation (mm)	Stiffness (N/mm)
1	161	5.03	2.28	23.4	19.7	2.57
2	160	4.95	2.19	22.6	18.0	2.64
3	160	5.12	2.43	23.1	19.6	2.42
4	162	5.08	2.29	23.1	18.7	2.58
5	160	4.99	2.27	22.7	19.4	2.55
6	159	5.15	2.34	23.3	18.6	2.55
Mean	**160**	**5.05**	**2.30**	**23.0**	**19.0**	**2.55**
SD	1	0.08	0.08	0.3	0.7	0.07

Table 5.3.1b Mechanical properties of single ply, non-twisted Dacron™ yarn.

Sample Number	Yield Stress (MPa)	Yield Strain (%)	Max. Stress (MPa)	Max. Strain (%)	Modulus (GPa)
1	178	1.41	827	12.2	14.6
2	175	1.37	800	11.2	14.9
3	181	1.52	818	12.2	13.7
4	180	1.42	818	11.6	14.8
5	176	1.42	803	12.1	14.4
6	182	1.47	823	11.7	14.3
Mean	**179**	**1.44**	**815**	**11.8**	**14.5**
SD	3	0.05	11	0.4	0.4

Table 5.3.2a Material properties of double plies, twisted Dacron™ yarn. Yarn twisting length is 2.5 mm.

Sample Number	Gage Length (mm)	Yield Load (N)	Yield Elongation (mm)	Max. Load (N)	Max. Elongation (mm)	Stiffness (N/mm)
1	156	10.1	2.57	48.3	24.3	4.46
2	160	10.2	2.73	48.3	25.0	4.21
3	157	9.9	2.62	47.3	23.9	4.28
4	158	10.0	2.68	47.9	24.2	4.25
5	157	9.9	2.66	48.6	26.1	4.21
6	155	10.0	2.61	48.4	24.8	4.35
Mean	**157**	**10.0**	**2.65**	**48.1**	**24.7**	**4.29**
SD	2	0.1	0.06	0.5	0.8	0.10

Table 5.3.2b Mechanical properties of double plies, twisted Dacron™ yarn. Yarn twisting length is 2.5 mm.

Sample Number	Yield Stress (MPa)	Yield Strain (%)	Max. Stress (MPa)	Max. Strain (%)	Modulus (GPa)
1	178	1.65	853	15.6	12.3
2	179	1.71	853	15.6	11.9
3	174	1.67	836	15.2	11.9
4	177	1.69	846	15.3	11.9
5	174	1.69	859	16.6	11.7
6	177	1.69	856	16.0	11.9
Mean	**177**	**1.68**	**851**	**15.7**	**11.9**
SD	2	0.02	8	0.5	0.2

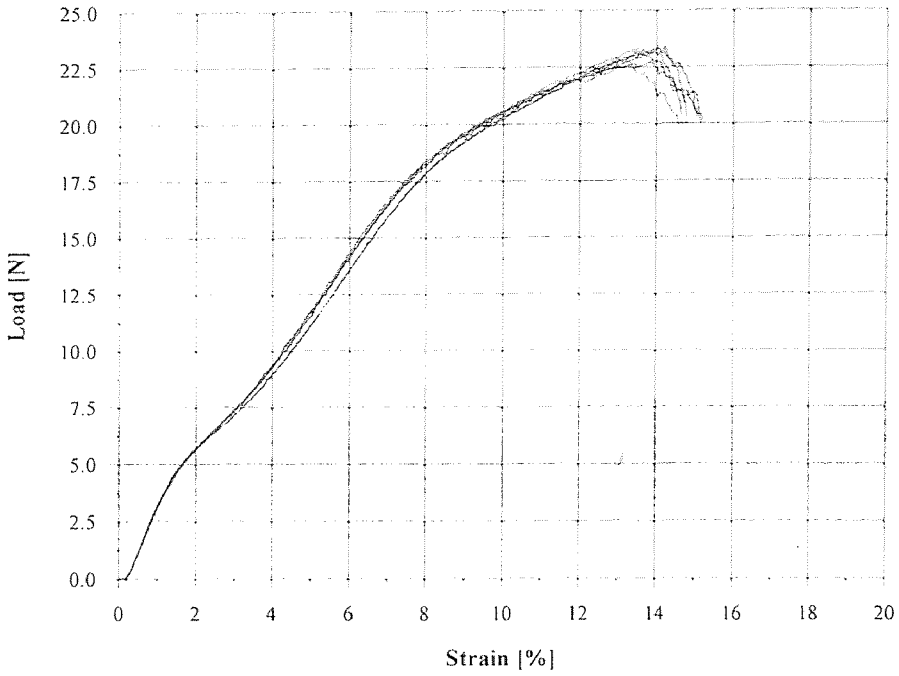

Figure 5.3.1 Load - Strain curves for single ply untwisted Dacron™ yarns.

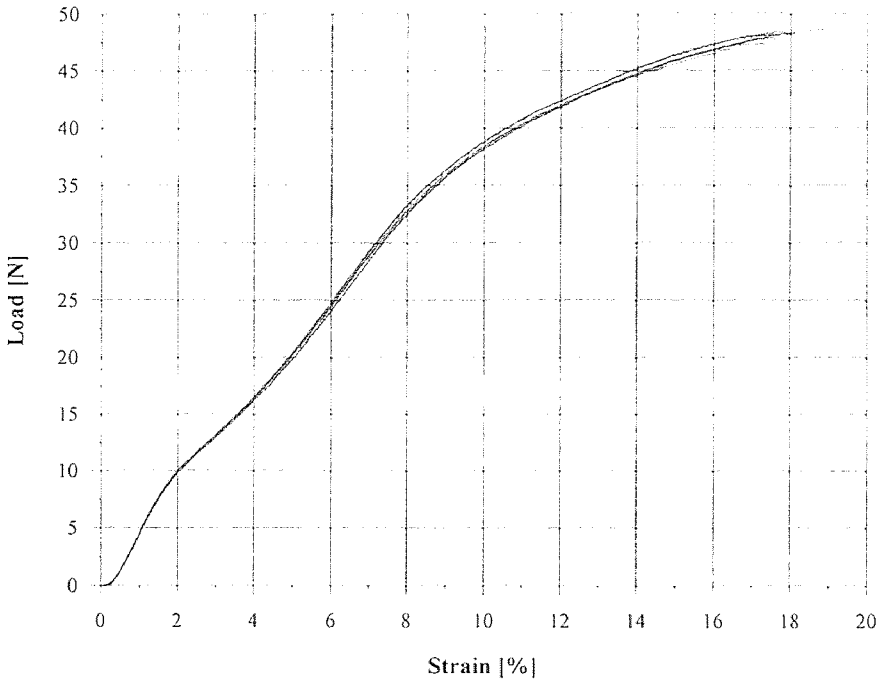

Figure 5.3.2 Load - Strain curves for double plies twisted Dacron™ yarns.

CHAPTER 6

DISCUSSION

6.1 Comparison of Truss and Beam Model of the Yarn Filament

From the present investigation, the truss element used for obtaining FEA results has shown its advantages in modeling of ligament yarn filaments. The shear stress of twisted filament is lower in comparison with the normal stress due to elongation (Figure 2.5.2). Moreover, the effect of bending on the normal stress is negligible (Figure 2.5.1). The normal stress generated by filament bending (beam model) is approximately less then 2% of normal stress from tensile loading. Also, the truss model of the ligament yarn filament has lower degrees of freedom in each node and it is easier to handle from the numerical point of view.

6.2 Contact Stress Elements

The filament which is subjected to the load P, lies on the edge of the yarn. It means that there are no additional forces acting on the filament. However, different loading condition is applied to the filaments which lie inside the yarn. These filaments are loaded from six sides (Figure 2.4.1). The stiffness of interconnecting elements, Hertzian contact, can be approximated from the result calculated from equation 3.1.7.

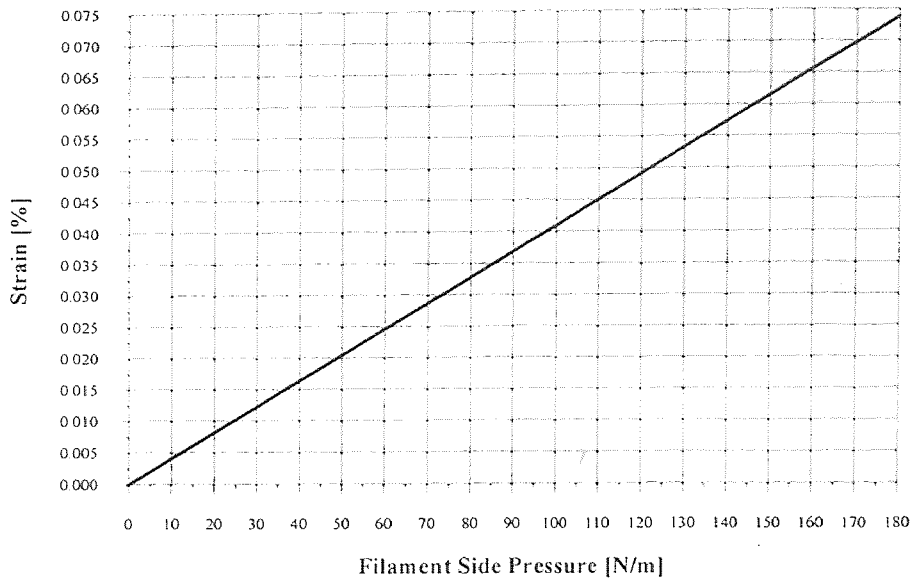

Figure 6.3.1 Filament side strain as a function of side pressure. The increase of side pressure was applied.

Despite the fact that the filament side contact pressure is greater than in some cases, for example, the maximum side pressure predicted in Section 3.3 (Figure 3.3.1), the stiffness of contact element did not change. The increase of side contact pressure from 45 [N/mm] to 180 [N/mm] obtained from finite element model (Figure 4.3.5) leads to a decrease of contact element stiffness from 243.66 [N/mm] to 243.57 [N/mm] (Figure 6.3.1). The change in contact element stiffness due to non-linearity of contact stiffness is, therefore, less then 0.04[%]. Hence, it also did not make any significant changes to the results obtained.

6.3 Finite Element Analysis

As it is predicted in the finite element analysis, there is a limitation in the domain of a solution. Extremely large or small elements cannot give satisfactory results. There is an

error in calculation of displacement and internal forces while using big size elements comparing to the model sizes. On the other hand, small element produces numerically unstable solution. The unstable solutions are due to finite binary number representation in computer memory, and a close to zero stiffness matrix determinant after applying boundary condition.

Considering convergence study performed in section 4.1, the smallest longitudinal element that gives convergent solution has a 5^0 element twisting angle. That angle is equivalent to, approximately, 34.7 [μm] in the element size (Figure 4.1.2).

There is a stress distribution between filaments. The filaments lied in the middle of the yarn carry higher load than the filaments lied on the yarn's outer boundary (Figure 4.1.3). The filament cross-section normal stress gradually decreases with the distance between yarn's and filament's symmetry axis increases. Filament to filament contact stress is distributed also. Similarly to the filament normal stress, the contact stress decreases with an increase of the distance between yarn's and filament's symmetry axis. In addition, the filament to filament contact stress also depends on the radial plane position regarding the filament to filament contact plane (Figure 4.1.5).

The linear dependency of external yarn strain due to internal forces is shown in section 4.2. The filament normal stress as well as contact stress is directly proportional to the yarn strain. This is due to the application of the linear truss element in the FEM.

As shown in Section 4.3, the yarn stiffness and its modulus depends on the yarn twisting length. The lower the twisting length, the smaller the stiffness and modulus (Figures 4.3.1 and 4.3.2). As the yarn twisting length decreases, starts from infinity, the

internal filament forces change their distribution. For the infinite twisting length, all filaments are parallel to each other, the normal stress perpendicular to the filament cross-section is equal.

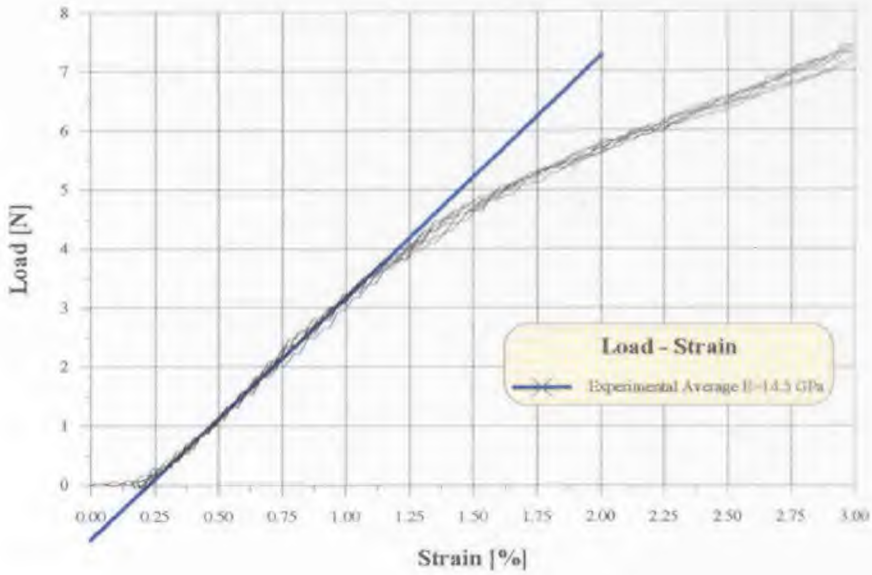

Figure 6.4.1 Load - strain curves for untwisted yarn, all filaments parallel

At this condition, there is no filament to filament contact stress. The lower the twisting length, the smaller the filament normal stress exerted on the filament that are lying on the yarn's boundaries. For twisting simulation conditions, the filaments that are lying in the middle section of the yarn, close to the yarn symmetry axis, carry more load and stress than the others (Figures 4.3.3, 4.3.4, 4.3.5, and 4.3.6). The highest load is carried by the filament lying on the symmetry axis.

Finally, the results obtained from the finite element analysis are confirmed by the experimental data (Figures 6.4.1 and 6.4.2). On each figure, the black curves represent

experimental data (Figures 3.3.1 and 3.3.2). The blue lines are the average strain - load curves calculated using the best fit method to experimental data. The red line that appeared on Figure 6.4.2 is the results using the finite element analysis for the yarn of 2.5 [mm] twisting length.

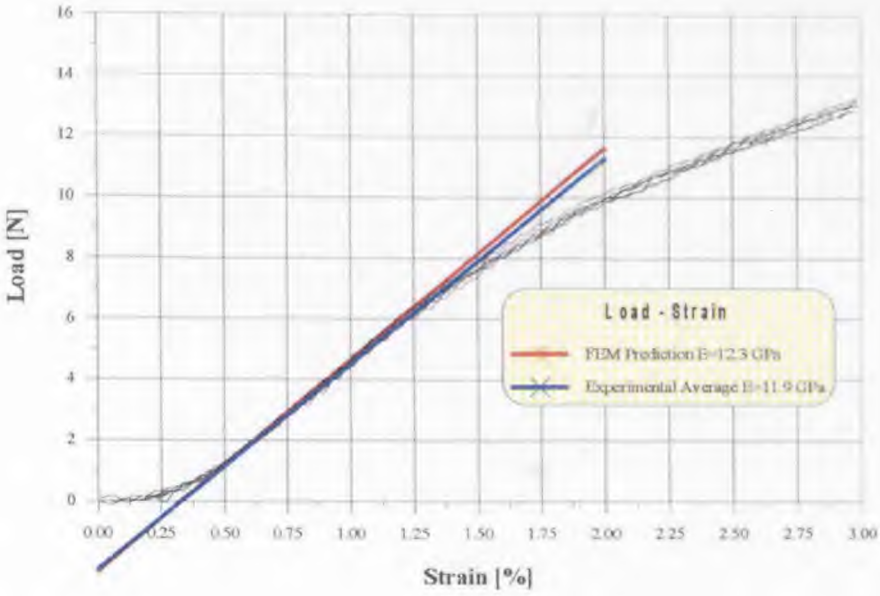

Figure 6.4.2 Load - strain curves for double plies twisted yarn, 2.5 mm twisting length.

6.4 Mechanical Properties of Dacron™ Yarns

The tensile test shows a significant difference in modulus and yield strain between non-twisted and twisted Dacron™ yarns. The average module for untwisted, single ply Dacron™ was 14.5±0.4 [GPa] (from experiment, Table 5.3.1b). On the other hand, the average modulus for double plies, twisted yarns with 2.5 [mm] twisting length was 11.9±0.2 [GPa] (Table 5.3.2b). The yield strain increased from 1.44±0.05 [%] for an untwisted, single ply Dacron™ yarn to 1.68±0.02 [%] for double plies, twisted yarns with 2.5 [mm] twisting

length. However, no difference in yield stress was observed. It was concluded that the drop in modulus for twisted yarns compared with the untwisted was contributed by the non-parallel orientation of filaments with respect to the yarn's symmetry axis of the untwisted yarns. In the twisted yarn, an oblique filament had to be align with the yarn symmetry axis before it could be deformed elasticity.

CHAPTER 7

CONCLUSION

7.1 Summary

The model used to predict stiffness, modulus, filament forces and stresses' distribution due to different yarn twisting lengths is successfully developed and analyzed. Yarns with lower twisting lengths were less stiffer than that of higher twisting lengths. From present investigation it can be summarized that the truss element for a FEM of a yarn is sufficient. It was shown that the beam model did not improve the results since the shear and bending moment of the filaments was relatively low. The optimal element size for a computational solution was determined in the convergence study. Too small in size of a finite element cause an instability in the solution. On the other hand, big elements cannot represent the spiral feature of the filament used in real life. Also, it was shown that the stress strain curve for the presented model was linear. This is due to assumption that the material properties are isotropic, linear, and homogenous. There is a direct agreement between experimental data and results obtained in the finite element analysis.

There are several findings of presented investigation. (1) Filament normal force and stress increase with an increase in strain (loading condition). (2) Filament normal force and stress decrease with an increase in the distance between the filament and yarn symmetry axis. (3) Filament normal force and stress increase with an increase in yarn twisting length (design parameter). (4) Filament contact force and stress increase with an

increase in strain. (5) Filament contact force and stress decrease with an increase in the distance between the filament and yarn symmetry axis. (6) Filament contact pressure and stress decrease with an increase in twisting length. (7) Yarn modulus and total force increase with an increase in twisting length.

7.2 Recommendations

The present model represents one step forward to the systematic stress analysis of on artificial ligament. In addition, the present analysis is the first step towards a complete understanding of the stress field using FEM, and provides the ground work for further non linear and dynamic analysis. The present model has provided important and useful information to the medical rehabilitation field. In the preparation of further work, the following steps will be considered in the modeling. (1) Change the material property from linear to quasi elastic nonlinear. (2) Apply viscoelestic material property. (3) Apply interfabric friction. (4) Apply filament length distribution. (5) The truss element can be used to model more complex system like artificial ligaments, tendons, arteries, and skin. (6) In addition, if each filament to be loaded to its limited force level, failure mode should be predicted.

APPENDIX A

LIGAMENT MESH GENERATION PROGRAM, C LANGUAGE

```
/*************************************************/
/*          Miroslaw Sokol                       */
/*                                               */
/*       Biomechanical Engineering               */
/*                                               */
/*          Master Thesis                        */
/*                                               */
/*       Last update:  7/29/94                   */
/*************************************************/

/*
This program was written to generate Finite Element Model of artificial ligament yarn.
This FEM model is based on few assumptions. First, each filament, of one yarn is a
neighbor of two to six other filaments. The filaments lying in the middle section of the
yarn have six neighbors filaments. The filament lying on the yarn boundary usually has
two to three neighbor filaments. As a filament model, truss element is lying in that
filament axis of symmetry. There is a full contact between filaments in the beginning of
loading process. The distributed contact force, normal to filament surface is conveyed by
```

desecrate mesh of elements that are orthogonal to filaments. Distributed contact force is modeled by using two concentrated nodal forces located on both ends of each longitudinal element.*/

```
/********************  PREPROCESSOR DIRECTIVES  ********************/

#include <stdio.h>
#include <math.h>
#include <string.h>
#include <malloc.h>

/************************ SYMBOLIC CONSTANTS ************************/
#define FALSE 0
#define TRUE  1
#define ABS(x) ((x) >= 0 ? (x) : -(x))

/************************  TYPE DECLARATIONS  ************************/

                                    /* Each node of this structure contains     */
 struct NODERC {                    /* ---------------------------------        */
  int       node_id;                /* node identification number               */
  double    x, y, z;                /* node coordinates x, y, z                 */
  double    length[6];              /* length of contact area                   */
```

```
  struct     NODERC  *next;              /* pointer to next node                */
  struct     NODERC  *neighbor[8];       /* [0..5] connection in plane          */
 };                                      /* [6..7] up and down connection       */

 typedef struct NODERC NODE;
 typedef NODE *PTNODE;

 struct LNTRC {
  int        lnt_id;
  double     length;
  struct     LNTRC  *next;
 };

 typedef struct LNTRC LNT;
 typedef LNT *PTLNT;

void main(argc, argv)
 int argc;
 char *argv[];
{
 PTNODE   joint, temp, front, back, up_front, up_temp;
 PTLNT    lnt=NULL, temp_lnt, found_lnt;
```

```
int     fiber_number = 15,          /* total number of filaments in the yarn      */
        substep_number = 4,         /* number of elements along the yarn          */
        node_on_radius;             /* number of nodes on the radius              */

static int sort[6]={3,4,5,0,1,2};

double  fiber_diameter = 1,         /* filaments diameter                         */
        fiber_length = 4,           /* yarn length                                */
        twisting_angle = 45,        /* total twisting angle in degrees            */
        substep_length,             /* longitudinal component of element length   */
        yarn_radius,                /* yarn radius                                */
        alpha,                      /* rotation angle in between layers           */
        beta,                       /* local twisting angle                       */
        displacement,               /* load in node displacenemt                  */
        pi = 4.*atan(1.),
        zero=0,
        temp_x, temp_y, temp_x0, temp_y0, temp_z0,
        xyr,
        det_x, det_y, det_z,
        l_temp, l_front,
        x, y, z, eps=1e-10;
```

```
int     ct, ctx, cty, ctz, ctn, max_x;

int     step, found;

FILE    *in, *nod, *elm, *cst;

double  get_data();

char    data[30], node[30], elem[30], cons[30], str[50];

printf("Start");

strcpy(data, argv[1]);
strcpy(node, argv[1]);
strcpy(elem, argv[1]);
strcpy(cons, argv[1]);
strcat(data, ".in");
strcat(node, ".nod");
strcat(elem, ".elm");
strcat(cons, ".cst");
```

```
if (argc < 2) {
  printf(" \nInput file name is not supplied");
  exit(1);
}

if ((in = fopen(data, "r")) == NULL) {
  printf(" \nCannot open data file");
  exit(1);
}

if ((nod = fopen(node, "w")) == NULL) {
  printf(" \nCannot open destination file");
  exit(1);
}

if ((elm = fopen(elem, "w")) == NULL) {
  printf(" \nCannot open destination file");
  exit(1);
}
```

```
if ((cst = fopen(cons, "w")) == NULL) {
 printf(" \nCannot open destination file");
 exit(1);
}

/* to read data parameters */
fiber_number   = get_data(in);
substep_number = get_data(in);
fiber_diameter = get_data(in);
fiber_length   = get_data(in);
twisting_angle = get_data(in);
displacement   = fiber_length*twisting_angle*get_data(in)/36000;

/* to calculate additional parameters */
temp_x = 1+4*(2*fiber_number/sqrt((double) 3) - 1)/3;
node_on_radius = (1. + sqrt(temp_x))/2. + 1.;
yarn_radius = (node_on_radius-1.)*fiber_diameter*sqrt((double) 3)/2;
fiber_length *= twisting_angle/360;
substep_length = fiber_length/substep_number;
temp_z0 = -1.*substep_length;
```

```
alpha = pi/180*twisting_angle/substep_number;

/* to calculate node coordinates */
back = NULL;
joint = NULL;
ct = 0;

printf( "\n  Calculate Node Coordinates");

for (ctz = 0; ctz <= substep_number; ++ctz) {
  temp_z0 += substep_length;
  temp_x0 = (2.-node_on_radius)*fiber_diameter/2;
  temp_y0 = node_on_radius*fiber_diameter*sqrt((double) 3)/(-2);
  max_x = node_on_radius-1;
  for (cty = 0; cty < 2*node_on_radius; ++cty) {
    step = (cty > node_on_radius) ? -1:1;
    temp_x0 -= step*fiber_diameter/2;
    temp_y0 += fiber_diameter*sqrt((double) 3)/2;
    temp_x = temp_x0 - fiber_diameter;
    temp_y = temp_y0;
    max_x += step;
    for (ctx = 0; ctx < max_x; ++ctx) {
```

```
temp_x += fiber_diameter;
xyr = sqrt(temp_x*temp_x + temp_y*temp_y);
if (xyr <= yarn_radius) {

  temp = (PTNODE) malloc(sizeof(NODE));
  temp->node_id = ++ct;
  temp->x = temp_x;
  temp->y = temp_y;
  temp->z = temp_z0;

  for (ctn = 0; ctn < 8; ++ctn)
    temp->neighbor[ctn] = NULL;
  temp->next = NULL;

  if (joint == NULL) {
    joint = temp;
    back = temp;
  } else {
    back->next = temp;
    back = temp;
  }
}
```

```
    }
  }
}

printf( " \n  Calculate Node Connections");

/* to calculate node connections */
temp = joint;
while (temp->next != NULL) {
 front = temp->next;
 while(front != NULL) {
  det_x = front->x - temp->x;
  det_y = front->y - temp->y;
  det_z = front->z - temp->z;
  if(ABS(det_x) + ABS(det_y) + ABS(det_z) > eps) {
   if (ABS(det_z) < eps) {
    found = FALSE;
    for (ctn = 0; ctn < 6 && !found; ++ctn) {
     x = det_x - fiber_diameter*cos(ctn*pi/3.);
     y = det_y - fiber_diameter*sin(ctn*pi/3.);
     if (ABS(x) < eps && ABS(y) < eps) {
      if (temp->neighbor[ctn] == NULL) {
```

```
            temp->neighbor[ctn]  = front;
            front->neighbor[sort[ctn]] = temp;
          }
          found = TRUE;
        }
      }
    } else if(ABS(det_x) < eps && ABS(det_y) < eps) {
      z = det_z/substep_length;
      if (ABS(z - 1) < eps) {
        if (temp->neighbor[6] == NULL) {
          temp->neighbor[6]  = front;
          front->neighbor[7] = temp;
        }
      } else if(ABS(z + 1) < eps) {
        if (temp->neighbor[7] == NULL) {
          temp->neighbor[7]  = front;
          front->neighbor[6] = temp;
        }
      }
    }
  }
front = front->next;
```

```
 }
 temp = temp->next;
}

printf( "\n  Rotate Node Coordinates");

/* to rotate nodes coordinates */
temp = joint;
while (temp != NULL) {
  beta =  alpha*temp->z/substep_length;
  det_x =  temp->x*cos(beta) + temp->y*sin(beta);
  det_y = -temp->x*sin(beta) + temp->y*cos(beta);
  temp->x = (ABS(det_x) > eps) ? det_x : 0;
  temp->y = (ABS(det_y) > eps) ? det_y : 0;
  temp = temp->next;
}

printf( "\n  Calculate Contact Length");

/* to rotate nodes coordinates */
temp = joint;
while (temp != NULL) {
```

```
for (ct = 0; ct < 6; ++ct) {
 if (temp->neighbor[ct] != NULL) {
  front = temp->neighbor[ct];

  if (temp->neighbor[6] != NULL)
   up_temp = temp->neighbor[6];
  else if (temp->neighbor[7] != NULL)
   up_temp = temp->neighbor[7];

  if (front->neighbor[6] != NULL)
   up_front = front->neighbor[6];
  else if (front->neighbor[7] != NULL)
   up_front = front->neighbor[7];

  det_x = temp->x - up_temp->x;
  det_y = temp->y - up_temp->y;
  det_z = temp->z - up_temp->z;
  l_temp = sqrt(det_x*det_x+det_y*det_y+det_z*det_z);

  det_x = front->x - up_front->x;
  det_y = front->y - up_front->y;
  det_z = front->z - up_front->z;
```

```
    l_front = sqrt(det_x*det_x+det_y*det_y+det_z*det_z);

    if ((temp->neighbor[6] != NULL) && (temp->neighbor[7] != NULL) )
      temp->length[ct] = (l_temp + l_front)/2;
    else
      temp->length[ct] = (l_temp + l_front)/4;
   }
  }
  temp = temp->next;
}

printf( "\n  Print Node Coordinates");

/* to print nodes coordinates */
temp = joint;
fprintf(nod, "%5d\n", -888);
while (temp != NULL) {
  fprintf(nod, "%5d", temp->node_id);
  fprintf(nod, "%16.9e", temp->x);
  fprintf(nod, "%16.9e", temp->y);
  fprintf(nod, "%16.9e", temp->z);
  temp_x = sqrt(temp->x*temp->x + temp->y*temp->y);
```

```
if (ABS(temp_x) > eps) {
 temp_x = temp->y/temp_x;
 temp_x = asin(temp_x)*180/pi;
 if ((temp->y >= 0) && (temp->x < 0))
  temp_x = 180 - temp_x;
 else if ((temp->y < 0) && (temp->x < 0))
  temp_x = 180 - temp_x;
 else if ((temp->y < 0) && (temp->x >= 0))
  temp_x = 360 + temp_x;
} else
 temp_x = 0;
fprintf(nod, "%9.4f", temp_x);
fprintf(nod, "%9.4f", zero);
fprintf(nod, "%9.4f", zero);
fprintf(nod, "\n");
temp = temp->next;
}

printf( "\n  Print Elements");

/* to print longitudinal elements */
temp = joint;
```

```
ctn = 0;
while (temp != NULL) {
  if (temp->neighbor[6] != NULL) {
     ++ctn;
     back = temp->neighbor[6];
     fprintf(elm, "%6d", temp->node_id);
     fprintf(elm, "%6d", back->node_id);
     for (ct = 0; ct < 6; ++ct)
       fprintf(elm, "%6d", 0);
     for (ct = 0; ct < 3; ++ct)
       fprintf(elm, "%6d", 1);
     fprintf(elm, "%6d", ctn);
     fprintf(elm, "%6d", 0);
     fprintf(elm, "  \n");
     temp->neighbor[6] = NULL;
     back->neighbor[7] = NULL;
   }
   if (temp->neighbor[7] != NULL) {
      ++ctn;
      back = temp->neighbor[7];
      fprintf(elm, "%6d", temp->node_id);
      fprintf(elm, "%6d", back->node_id);
```

```
    for (ct = 0; ct < 6; ++ct)
      fprintf(elm, "%6d", 0);
    for (ct = 0; ct < 3; ++ct)
      fprintf(elm, "%6d", 1);
    fprintf(elm, "%6d", ctn);
    fprintf(elm, "%6d", 0);
    fprintf(elm, "  \n");
    temp->neighbor[7] = NULL;
    back->neighbor[6] = NULL;
  }
  temp = temp->next;
}


temp_lnt = (PTLNT) malloc(sizeof(LNT));
temp_lnt->lnt_id = 1;
temp_lnt->length = pi*fiber_diameter*fiber_diameter/4;
temp_lnt->next = lnt;
lnt = temp_lnt;


/* to print contact elements */
```

```
cty = 1;
temp = joint;
while (temp != NULL) {
  for (ctx = 0; ctx < 6; ++ctx) {
    if (temp->neighbor[ctx] != NULL) {

      found = 0;
      temp_lnt = lnt;
      while ((temp_lnt != NULL) && !found )
        if (ABS(temp_lnt->length - temp->length[ctx]) < eps)
          found = 1;
        else
          temp_lnt = temp_lnt->next;

      if (!found) {
        ++cty;
        temp_lnt = (PTLNT) malloc(sizeof(LNT));
        temp_lnt->lnt_id = cty;
        temp_lnt->length = temp->length[ctx];
        temp_lnt->next = lnt;
        lnt = temp_lnt;
      }
```

```
    ++ctn;
    back = temp->neighbor[ctx];
    fprintf(elm, "%6d", temp->node_id);
    fprintf(elm, "%6d", back->node_id);
    for (ct = 0; ct < 6; ++ct)
      fprintf(elm, "%6d", 0);
    for (ct = 0; ct < 2; ++ct)
      fprintf(elm, "%6d", 2);
    fprintf(elm, "%6d", temp_lnt->lnt_id);
    fprintf(elm, "%6d", ctn);
    fprintf(elm, "%6d", 0);
    fprintf(elm, "  \n");
    temp->neighbor[ctx]   = NULL;
    back->neighbor[sort[ctx]] = NULL;
   }
  }
 temp = temp->next;
}


printf( "\n  Print Real Constance Table\n\n");
```

```
fprintf(cst, "/show,x11\n");
fprintf(cst, "/prep7\n");
fprintf(cst, "et,link,8\n");
fprintf(cst, "et,link,8\n");
fprintf(cst, "mp,ex,1,4452\n");
fprintf(cst, "mp,ex,2,%f\n", 74.7*fiber_diameter);
fprintf(cst, "nread,%s,nod\n", argv[1]);
fprintf(cst, "eread,%s,elm\n", argv[1]);

temp_lnt = lnt;
while (temp_lnt != NULL) {
  fprintf(cst, "R,");
  fprintf(cst, "%d,", temp_lnt->lnt_id);
  fprintf(cst, "%g", temp_lnt->length);
  fprintf(cst, "\n");
  temp_lnt = temp_lnt->next;
 }

temp = joint;

fprintf(cst, "D,all,uy,0\n");
```

```
while (temp != NULL) {
 if (ABS(temp->z) < eps) {
  fprintf(cst, "D,");
  fprintf(cst, "%d,", temp->node_id);
  fprintf(cst, "uz,0");
  fprintf(cst, "\n");
  if ( ABS(temp->x) < eps && ABS(temp->y) < eps) {
   fprintf(cst, "D,");
   fprintf(cst, "%d,", temp->node_id);
   fprintf(cst, "ux,0");
   fprintf(cst, "\n");
  }
 }
 if (ABS(temp->z - fiber_length) < eps) {
  fprintf(cst, "D,");
  fprintf(cst, "%d,", temp->node_id);
  fprintf(cst, "uz,");
  fprintf(cst, "%f", displacement);
  fprintf(cst, "\n");
 }
 temp = temp->next;
}
```

```
fprintf(cst, "eplot\n");
fprintf(cst, "finish\n");
fprintf(cst, "/SOLU\n");
fprintf(cst, "ANTYPE,STAT,NEW\n");
fprintf(cst, "SOLVE\n");
fprintf(cst, "FINISH\n");
fprintf(cst, "/POST1\n");
fprintf(cst, "etable,axial,epel,1\n");
fprintf(cst, "etable,memfor,smisc,1\n");
fprintf(cst, "/output,%s,mfo\n", argv[1]);
fprintf(cst, "pretab\n");
fprintf(cst, "/output,\n");
fprintf(cst, "finish\n");
fprintf(cst, "/exit");

fclose(in);
fclose(nod);
fclose(elm);
fclose(cst);
}
```

```
double get_data(input)
FILE *input;
{
  char buffer[256];

  fgets(buffer, 256, input);
  buffer[10] = '\0';
  return atof(buffer);
 }
```

BIBLIOGRAPHY

1. Woo, S. L-Y., Johnson, G. A. & Smith, B. A., Mathematical Modeling of Ligaments and Tendons. *The 20th Anniversary of the American Society of Mechanical Engineers Biomechanics Symposium, Breckenridge, CO*, (June 25-29, 1993) 468-473.

2. Funk, F. J. Jr. MD, General Orthopedics - Synthetic Ligaments Current Status. *Clinical Orthopedics and Related Research*, (1986): 107-111.

3. Schepsis, A. A. MD & Greenleaf, J. MD, Prosthetic Materials for Anterior Cruciate Ligament Reconstruction. *Orthopedic Review*, **XIX-11** (1990) 984-991.

4. Girgis, F. G. MD, Ph.D., Marshall, J. L. D.V.M., MD & Monajem A.R.S., MD, The Cruciate Ligaments of the Knee. *Clinical Orthopedics and Related Research* **106** (1975) 216-231.

5. Fujikawa, K., Ohtani, T., Matsumoto, H. & Seedhom, B.B., Reconstruction of the Extensor Apparatus of the Knee with Leeds-Keio Ligament. *British Editorial Society of Bone and Joint Surgery*, **76-B** (1994) 200-203.

6. Frisen, M., Magi, M., Sonnerup, L. & Viidik, A., Rheological Analysis of Soft Collagenous Tissue. Part I: Theoretical Consideration. *Journal of Biomechanics* **2** (1969) 13-20.

7. Stouffer, C. D., Butler, D. L. & Hosny, D., The Relationship Between Crimp Pattern and Mechanica Responce of Human Patellar Tendon Bone Units. *ASME Journal of Biomechanical Engineering*, **107** (1985) 158-165.

8. Belkoff, S. M. & Haunt, R. C., A Structural Model Used to Evaluate the Changing Microstructure of Maturing Rat Skin. *Journal of Biomechanics*, **24-8** (1991) 711-720.

9. Sidles, J. A., Clark, J. M. & Garbini, J. L., A Geometric Theory of the Equilibrium Mechanics of Fibers in Ligaments and Tendons. *Journal of Biomechanics*, **24-10** (1981) 943-949.

10. Noyes, F. R., DeLucas, J. L. & Torvik, P. J., Biomechanics of Anterior Cruciate Ligament Failure: an Analysis of Strain-rate Sensitivity and Mechanics of Failure in Primates. *Journal of Bone and Joint Surgery*, **56A** (1974) 236-253.

11. Noyes, F. R. & Grood, E. S. The Strength of the Anterior Cruciate Ligament in Humans and Rhesus Monkeys. Age-related and Species-related Changes. *Journal of Bone and Joint Surgery*, **58A** (1976) 1074-1082.

12. Oberg, E., Franklin, D. J., Holbrook, L. H. & Ryffel H. H., *Machinery's Handbook*, **24** edition (1992) 167.

13. Kennedy LAD Ligament Augmentation Device. *Minnesota Mining and Manufacturing Company*, (1987) 1-25.

14. Stryker Dacron™ Ligament Prosthesis Surgical Technique. *Meadox Medical Inc.*, (Oakland 1983) 1-10.

15. Amis, A. A., Kempson, S. A., Campbell, J. R. & Miller, J. H., Anterior Cruciate Ligament Replacement - Biocompatibility and Biomechanics of Polyester and Carbon Fiber in Rabbits. *British Editorial Society of Bone and Joint Surgery*, **70B** (1988) 628-634.

16. Blankevoort, L. & Huiskes, Ligament-Bone Interaction in a Three-Dimensional Model of the Knee. *Journal of Biomechanical Engineering*, **113** (1991) 263-269.

17. Claes, L., Durselen, L., Kiefer, H. & Mohr, W., The Combined Anterior Cruciate and Medial Collateral Ligament Replacement by Various Materials: A Comparative Animal Study. *Journal of Biomedical Materials Research: Applied Biomaterials*, **21-A3** (1987) 319-343.

18. Dandy, D. J. & Gray, A.J.R., Anterior Cruciate Ligament Reconstruction with the Leeds-Keio Prosthesis Plus Extra-Articular Tenodesis. *British Editorial Society of Bone and Joint Surgery*, **76-B-2** (1994) 193-197.

19. Demmer, P., Fowler, M. & Marino A. A., Use of Carbon fiber in Reconstruction of Knee Ligaments. *Clinical Orthopedics and Related Research*, (1991) 225-232.

20. Kastelic, J., Palley, I. & Baer, E., A Structural Mechanical Model for Tendon Crimping. *Journal of Biomechanics*, **13** (1980) 887-893.

21. Padavin, J., Parris H. & Ma, J., Large Deformation Micropolar Theory for Cord Rubber Composites. *Rubber Chemistry and Technology*, **68** (1995) 1-20.

22. Peterson, C. J., Donachy, J. H. & Kalenak, A., A Segmented Polyurethane Composite Prosthetic Anterior Cruciate Ligament in vivo Study. *Journal of Biomedical Materials Research*, **19** (1985) 589-594.

23. Stouffer, C. D., Butler, D. L. & Hosny, D., The Relationship Between Crimp Pattern and Mechanical Response of Human Patellar Tendon-Bone Units. *The American Society of Mechanical Engineers Journal of Biomechanical Engineering*, **107** (1985) 158-165.

24. Takakuza, K., Fujii, S., Miyairi, H., Koizumi, T. & Muneta, T., Mechanical Problems in the Reconstruction of Anterior Cruciate Ligaments - Mechanical Compatibility between Living Tissue and Artificial Materials. *JSME International Journal*, **36-A-3** (1993) 327-332.

25. Thomas, N. P., Turner, I. G. & Jones, C. B., Prosthetic Anterior Cruciate Ligaments in the Rabbit. *British Editorial Society of Bone and Joint Surgery, the Journal of Bone and Joint Surgery*, **69-B-2** (1987) 312-316.

26. Woods, W. G. MD, Synthetics in Anterior Cruciate Ligament Reconstruction: A Review. *Orthopedic Clinics of North America* **16-2** (1985) 227-235.